UCL Université catholique de Louvain

École polytechnique de Louvain (EPL)

epl

Numerical study of whitings formation on the Bahama Banks

Dissertation presented by
Thomas DOBBELAERE

for obtaining the Master's degree in
Mathematical Engineering

Supervisor(s)
Emmanuel HANERT, Éric DELEERSNIJDER

Reader(s)
Jonathan LAMBRECHTS, Sam PURKIS

Academic year 2017-2018

Acknowledgments

My first thanks go to my supervisor Emmanuel Hanert. Prof. Hanert was always available to answer my questions or check my (last minute) results and it has been a real pleasure to work under the dedicated supervision of someone with such a helpful and optimistic character. I also thank my co-supervisor Éric Deleersnijder.

I would then like to thank Valentin Vallaeys, David Vincent, Antoine Saint-Amand and Jonathan Lambrechts, who kindly guided me in the code jungle of SLIM. They helped me debugging my codes all along the modeling process and even developed some model features for me. They are the computer wizards who made this master thesis possible.

I would also like to thank Matthieu le Hénaff, Mohamed Iskandarani, Sam Purkis, Amanda Oehlert and their colleagues who kindly welcomed us in Florida. I especially thank Sam Purkis and Amanda Oehlert for the help they gave me for the geological part of the study and for their enthusiastic feedbacks; it truly was rewarding and motivating.



My final thanks go to kot Erasmus teams. Even though they made me lose some precious work time to some less serious activities, they have been an immeasurable support for three years now, especially when they were asking this fateful question: "T'as toujours pas fini ton mémoire !?".

Contents

1 Introduction **1**

1.1 The Bahama Banks . . . 1

1.2 About whitings . . . 1

1.3 Existing models for whitings formation . . . 2

1.3.1 Biological mediation . . . 2

1.3.2 Direct precipitation . . . 4

1.3.3 Resuspension . . . 5

1.4 Objective . . . 6

2 Currents simulation on the Bahamian Bank **7**

2.1 Hydrodynamic model . . . 7

2.2 Unstructured mesh . . . 9

2.3 Model forcings . . . 10

2.4 Validation of the hydrodynamics . . . 11

2.5 Wetting-drying . . . 14

2.6 Limitations . . . 17

3 Designing indicators to study whitings **18**

3.1 Bottom sediment resuspension indicators: threshold and mean velocity . . . 18

3.1.1 Impact of the slope-dependent friction parameter . . . 19

3.1.2 Mean and standard deviation of the velocity . . . 19

3.2 Water chemistry indicators . . . 20

3.2.1 Tracking of water mixing . . . 20

3.2.2 Mean volume flow rate through the 30m isobath . . . 22

3.2.3 Water age . . . 22

4 Basic shallow water equations: results **24**

4.1 Resuspension indicators . . . 24

4.2 Water chemistry indicator . . . 28

4.2.1 Lagrangian Particle Tracker . . . 28

4.2.2 Mean volume flow rate through the 30m isobath . . . 30

4.2.3 Age of waters . . . 31

4.2.4 Water chemistry indicators: summary . . . 31

5 Wetting-drying: results **34**

5.1 Resuspension indicators . . . 34

5.2 Water chemistry indicators . . . 37

5.2.1 Lagrangian Particle Tracker . . . 37

5.2.2 Mean volume flow rate through the 30m isobath 38
5.2.3 Age of waters 39
5.2.4 Wetting-drying without slope-dependent friction 39
5.2.5 Water chemistry indicators: summary 42

6 Conclusion **43**

A Appendices **51**

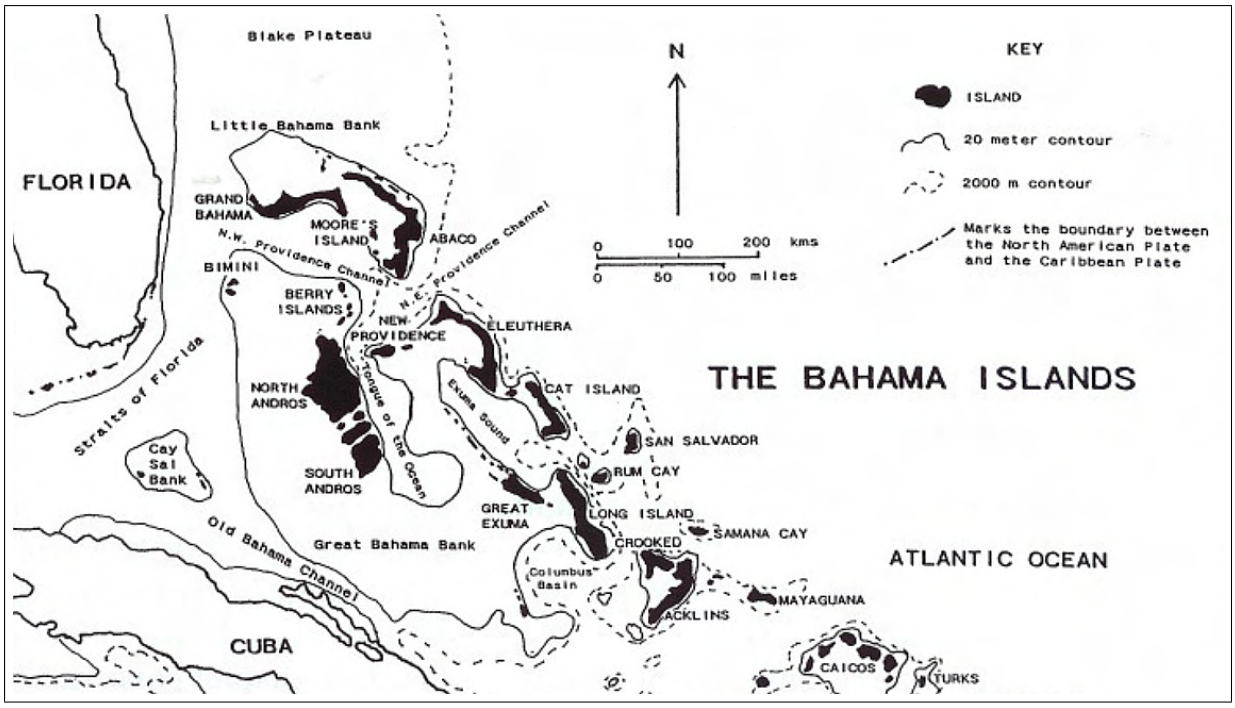

Fig. 1.1: Map of the Bahamas from [Carew and Mylroie, 1995]

1 Introduction

1.1 The Bahama Banks

The Bahamian archipelago mainly consists of two carbonate banks, the Great Bahama Bank (GBB) and the Little Bahama Bank (LBB), covering altogether a total area of about 300 000 km^2 [Meyerhoff and Hatten, 1974]. These banks are for the most part shallower than 10 m deep and are bounded by near-vertical slopes into deep water. The Great Bahama Bank is embayed by two deep troughs: Tongue of the Ocean (TOTO) in the center and Exuma Sound to the east. Its largest island is the Andros Island, whose eastern coasts are boarding the Tongue of the Ocean. The Great Bahama Bank also counts the Berry Islands, north to Andros and the Bimini Islands, at the northwestern tip of the bank. Little Bahama Bank and Great Bahama Bank are separated by Northwest Providence Channel (north to Bimini Island) and Northeast Providence Channel. The main islands of the LBB are Abaco and Grand Bahama Islands.

Marine waters of Bahamas have average temperature ranging from 18°C (winter: November 1st to April 30th) to 28°C (summer: May 1st to October 31st). The Antilles Current brings water to the Bank from the southeast. This current divides into two flows, one going northwestward along the eastern margin of the archipelago and another one going northwestward through Old Bahama Channel, on the southwestern margin of the Great Bahama Bank. The Bahama banks are boarded on the west by the Florida Strait and the Gulf Stream, flowing northward.

1.2 About whitings

The Great Bahama Bank, as a flat-topped, isolated carbonate platform, is at the origin of much understanding about processes of carbonate sedimentation and geological models [Harris et al., 2015]. Among geological phenomena of interest occurring on this platform are lime mud production and distribution, that could help us understanding the role of carbonate within atmospheric and oceanic carbon reservoir [Milliman and Droxler, 1995]. In this context, one

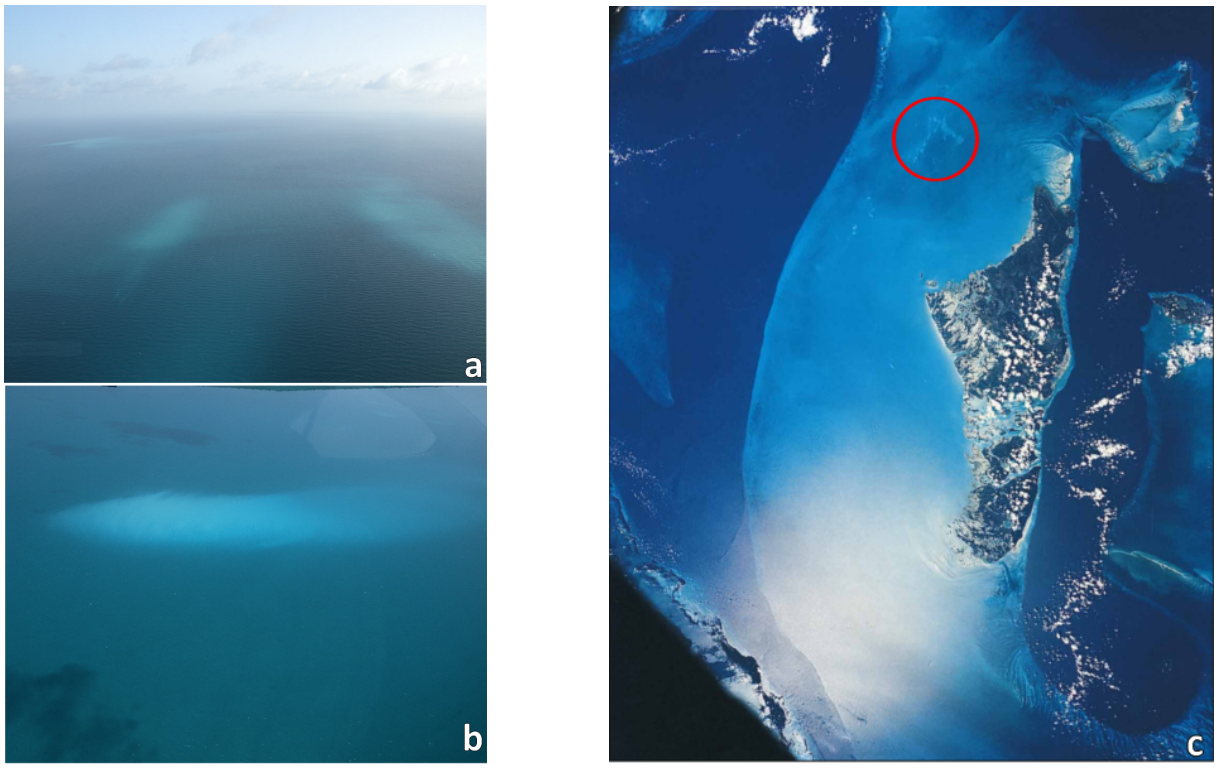

Fig. 1.2: Examples of whitings. Photograph **a** has been taken 20 June 2013 about 25km west of Marsh Harbor and shows whitings of about 1 km long. Photograph **b** has been taken 19 June 2013 in the Marls of Abaco [Larson and Mylroie, 2014].

of the main questions is the origin of most of the carbonate mud on the GBB. It is currently thought that between 25% and 50% of the mud are aragonite ($CaCO_3$) needles resulting from calcareous green algae decomposition [Bathurst, 1972; Milliman et al., 1993] while the remaining 50-75 % is expected to originate from inorganic and/or bio-induced *whitings* [Shinn et al., 1989].

Whitings are drifting patches of fined-grained aragonite observed on the Bahama Banks (see figure 1.2), with an average estimate of 70 km^2 of daily whitings area. Most of them ($75\% - 80\%$) occur in the region around lat $25°N$ and $78°50'W$, in the north-central part of western GBB, which exhibits a mud and pellet-mud facies (see figure 1.3).
Moreover, temporal distribution of whitings seem to have a seasonal component with higher occurrence frequencies in April and October and lower occurrence frequencies January, March, May, June, July, August and September (see figure 1.4); with each individual whiting having a lifespan going from days to weeks [Shinn et al., 1989].

However, whitings have been a sedimentological enigma for the last 80 years and explanation of their formation mechanism is still controversial. We will thus present in the next section a quick review of the existing models.

1.3 Existing models for whitings formation

1.3.1 Biological mediation

This first model is the newest mechanism proposed to explain whitings formation. In this framework, four different mechanisms are suspected to cause whitings apparition: picoplankton blooms [Robbins and Blackwelder, 1992], phytoplankton blooms [Wells and Illing, 1964], green algae [Yates and Robbins, 1998] and aragonite growth in microbes extracellular substances

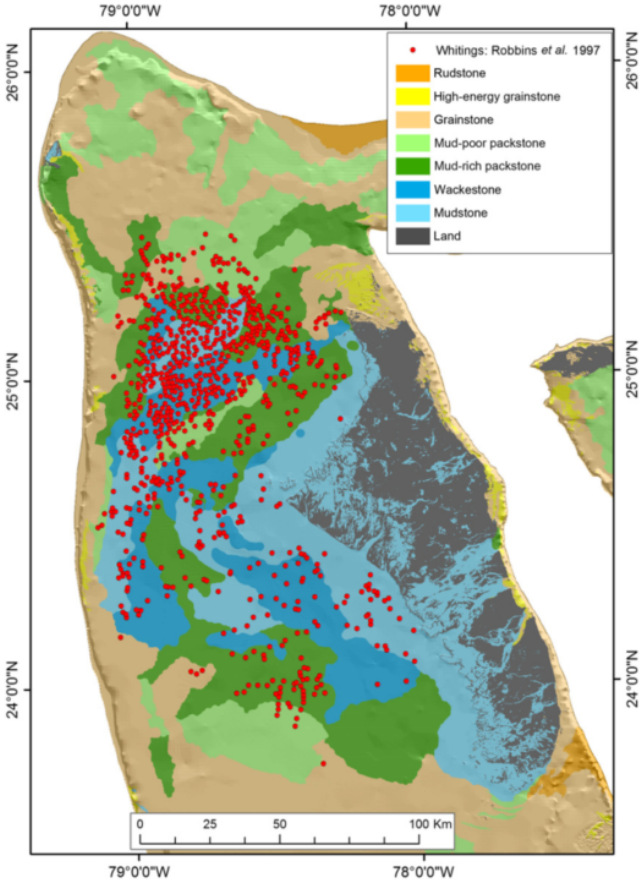

Fig. 1.3: Spatial distribution of whitings compiled by [Robbins et al., 1997] on the depositional facies map of [Harris et al., 2015]

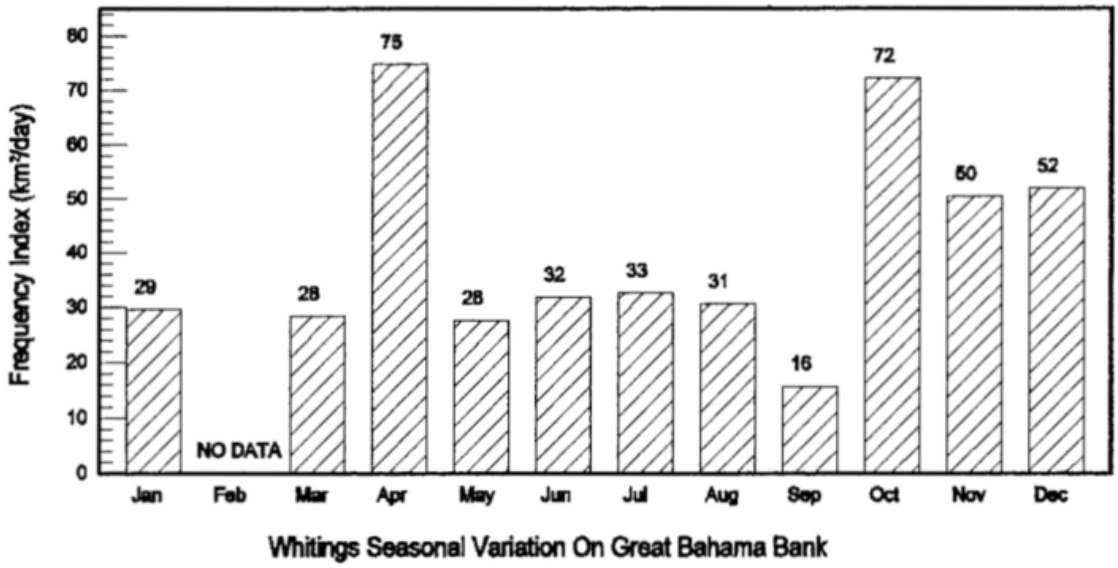

Fig. 1.4: Temporal distribution of whitings compiled by [Robbins et al., 1997] with the frequency index being defined as $\frac{\text{sum of whitings area/month}}{\text{mission days}}$

[Thompson, 2000].

The first mechanism is supported by the fact that about 25% of the solid weight of the whitings is made up of organic matter and that adjacent clear waters have a lower organic (e.g. picoplankton) content. Moreover, scanning electron microscopy analysis of whitings samples revealed that they were containing $1 - 30\mu m$ long organic structures covered with cristal of aragonite or calcite. Based on these evidences, [Robbins and Blackwelder, 1992] suggested that calcium carbonate precipitation could be induced by algal cells as photosynthetic picoplankton remove CO_2 from water.

The second mechanism is based on the study of whitings in the Persian Gulf. [Wells and Illing, 1964] observed a five- to tenfold increase in plankton populations inside whitings. Persian Gulf waters usually being saturated with aragonite, a sharp increase in carbone dioxyde consumption due to a sudden increase in phytoplankton populations would then easily incur precipitation in order to restore chemical equilibrium. However, Persian Gulf waters are much more nutrient rich that the ones of the Bahamas.

The third mechanism is based on the investigation of the ability of the unicellular green alga *Nannochloris atomus* to precipitate $CaCO_3$ [Yates and Robbins, 1998]. It appears that a density of 10^5 cells/mL of *N. atomus* (which is consistent with measurements made in Bahamian whitings [Robbins et al., 1996]) can yield a calcification value of 1.55 mg/L in 12 hour, which in a water volume of $3.2 \cdot 10^9$ L results in a production of $5 \cdot 10^3$ kg of $CaCO_3$ per day. These values are comparable to $CaCO_3$ sediment yield from Bahamian whitings.

Finally, the fourth and last mechanism is based on the role played by a bacteria (*Synechococcus*) in an annual whiting event in Fayetteville Green Lake (FGL) in upstate New York. In this model, calcite precipitates in the micro-environment surrounding the cell via surface binding and calcium excretion from the cell, because of elevate pH and higher Ca^{++} concentration. Due to fractionation of ^{12}C by the cell, the precipitated calcite in enriched in ^{13}C. Such a ^{13}C enrichment is also observed in marine whitings carbonate and bottom sediment [Shinn et al., 1989], which would suggest a bacterial fractionation process similar the one occurring in the FGL. However, such a process would involve some form of complex biophysicochemical coupling in the case of the GBB.

However, there are some evidence against biological mediation. First, bank-top waters seem to have very low concentration of essential nutrients for large colonies of organisms. Then, rapid photosynthetic uptake within blooms would incur a large p_{CO_2} depletion, which has never been observed. Finally, ^{14}C measurements of whitings particles and grain morphology of whiting materials are inconsistent with grains produced by organisms.

1.3.2 Direct precipitation

A second potential mechanism for whitings formation is the direct precipitation of aragonite, related to the water saturation Ω with respect to $CaCO_3$, given by:

$$\Omega = \frac{\left[Ca^{2+}\right]\left[{CO_3}^{2-}\right]}{K^*_{sp}} \tag{1.1}$$

where K^*_{sp} is the apparent solubility product of aragonite at given salinity, pressure and temperature and $[Ca^{2+}]$ and $[{CaCO_3}^{2-}]$ are the calcium and carbonate ions concentrations. When water gets super-saturated with respect to aragonite ($\Omega > 1$), precipitation occurs until water is no longer super-saturated. The rate R of this precipitation is given by the following

empirical formula [Mucci and Morse, 1983]

$$R = k(1 - \Omega)^n \tag{1.2}$$

where k is a rate constant and n is the empirical reaction order. According to 1.1, aragonite saturation state depends thus on water salinity ($[Ca^{2+}]$ increases with salinity) and atmospheric CO_2 concentration. Indeed, when CO_2 enters water, a fraction of the dissolved carbone dioxyde reacts with water to form carbonic acid H_2CO_3. Some of this acid then dissociates, producing hydrogen ions H^+ and bicarbonate ions HCO_3^-. Finally, some of the generated H^+ combine with carbonate ions CO_3^{2-} to form more HCO_3^- [Jiang et al., 2015]. This process is synthesized in the following global equation:

$$CO_2 + H_2O + CO_3^{2-} \rightleftharpoons 2\,HCO^- \tag{1.3}$$

Therefore, increase of the atmospheric CO_2 concentration decreases aragonite saturation state [Kuchinke et al., 2014]. Finally, one can note that aragonite saturation rate decreases with water residence time on the GBB, and therefore (counter-intuitively) with salinity [Broecker et al., 2001]

Since bank waters of the Bahamas are often super-saturated with $CaCO_3$, this model seems to be a reasonable mechanism for the formation of whitings. However, studies on $CaCO_3$ precipitation kinetics [Morse et al., 2003] brought some strong evidence against direct, pseudo-homogeneous precipitation.
First, $CaCO_3$ precipitation is associated with a decrease of water alkalinity. However, no important change in water alkalinity has ever been observed in the whitings of the Great Bahama Bank (even though such decrease has been measured in the Little Bahama Bank [Bustos-Serrano et al., 2009]). Moreover, as in the biological mediation model, direct precipitation cannot explain the old ^{14}C age of the whiting grains.

These 2 drawbacks lead us to the *hip-hop'n* model, in which fine grained sediments are resuspended (by an unstated mechanism) and serve then as nucleation points for aragonite precipitation. Such a model would be in accordance with ^{14}C data. Furthermore, with such a model, the precipitation of $CaCO_3$ on resuspended material would only incur a decrease of $\approx 0.5\%$ of water alkalinity.
However, this model cannot explain the ^{7}Be age distribution measured on the whiting grains.

1.3.3 Resuspension

As seen in the previous section, resuspension of the bottom sediments is likely to play an important role in the mechanism of whitings formation. However, there is currently no accepted model explaining this resuspension process. The different models that have been proposed until now are listed below.

A first model is the resuspension due to fish activities. Some have hypothesized that bottom-sediment resuspension could be due to bottom-feeding fishes extracting edible components from the sediments and ejecting the remaining fine-grained sediments into water column. On the other hand, others have proposed that black-tipped sharks could use suspended sediments to trap their preys [Broecker et al., 2000]. These two theories seem pretty unlikely since schools of fishes large enough to explain the important number and area of whitings have never been observed in the Great Bahamas Bank.

A second model is resuspension due to micro-turbulent bursts [Boss and Neumann, 1993], which are due to the transition of the flow regime on the bank from laminar to turbulent. The interest of this model is that observed physical characteristics of whitings are consistent with predicted and observed patterns of turbulent-flow systems (e.g. roiling nature, digitate

turbidity, ...). Nevertheless, this hypothesis has never been tested on the bank and is based on computer modeling only.

A third model is resuspension due to Langmuir circulation [Zimmerman et al., 2009]. This kind of circulation is usually made up of a pair of parallel counter-rotating cells oriented in the downwind direction, caused by the interaction between wind-driven shear current and the Stokes drift current from surface gravity waves. This model is consistent with the temporal pattern of whitings.

Nevertheless, although resuspension hypothesis are supported by ^{14}C datation, no model has been able to satisfactorily explain how resuspension occurs until now. Moreover, ^{7}Be data and grain morphologies of whiting do not match the ones of the bottom-sediment.

Finally, a last and pretty recent model for the formation of whitings are the infilled blue holes [Larson and Mylroie, 2012]. Blue holes are subsurface voids developed in carbonate banks and islands. They're tidally active with strong inflow and outflow currents. Moreover, they are usually linked to lateral conduits of fracture guided passages. In this model, water in sediment-filled blue holes is raised to bank top due to tidal pumping. Because of depth pressure, deep water contains more CO_2 than bank water. Hence when deep-seated water rises to the bank top, it degases and warms, which drives precipitation of $CaCO_3$. Although this model would be consistent with the physical properties of the whitings, it is based on an extrapolated distribution of the blue holes. Furthermore, we have no proof that these extrapolated sediment-filled blue holes are connected to conduits just as the "classic" ones.

1.4 Objective

As seen in the previous section, none of the different models taken separately are able to explain whitings formation in a satisfactory manner. The underlying mechanisms must result from an intricate bio-physico-chemical coupling between microbial communities, water circulation and chemistry. The present paper does not aim at bringing a final answer to the whitings enigma but tends on the other hand to bring some new insight on the question via high-resolution hydrodynamics modeling on the Great Bahama Bank. To do so, the following steps must be achieved:

1. A high-resolution ocean model must be devised for water circulation on Great Bahama Bank.
2. Indicators must then be developed in order to extract relevant information from the current simulations in the context of whitings.
3. Information of the developed indicators must finally be compared with whitings occurrence and therefore confirm or infirm a possible relationship between hydrodynamics and areas with enhanced whiting production.

The developed model and the information extracted from it could then used in further research on whitings formation mechanism.

2 Currents simulation on the Bahamian Bank

In order to simulate the currents on the Bahamian Banks, we use SLIM[1] as hydrodynamic model. SLIM is a numerical ice-ocean model developed at the Université Catholique de Louvain (UCL) in order to solve equations governing geophysical, environmental and groundwater phenomena by means of discontinuous Galerkin finite element method on 1D, 2D or 3D unstructured meshes. Such a discontinuous finite-element method has been proved to be among others pretty efficient for solving shallow water flows [Aizinger and Dawson, 2002; Schwanenberg and Harms, 2004; Remacle et al., 2006]. It combines the advantages of both continuous finite-element methods and finite volumes and is known to be especially efficient for hyperbolic conservation laws [Cockburn and Shu, 2001] and robust solutions are known to handle second-order diffusive operators [Riviere, 2008]. Moreover, due to the discontinuous character of the solution, parallel implementation is pretty straightforward [Bernard et al., 2007].
Finally, SLIM has already been successfully applied on several coastal oceans and estuaries around the world [Lambrechts et al., 2008; Le Bars et al., 2016; De Brye et al., 2010; de Brye et al., 2011] and even on the Saturnian moon Titan [Vincent et al., 2016].

In the context of this study, we used the 2D barotropic version of SLIM, which models horizontal depth-integrated velocities. This simplification of the physics of our problem allowed us to perform simulations at a very high resolution of about 1 km on the whole Bahama bank, which has never been performed before.

This section will discuss about the calibration, validation and limitations of our hydrodynamic model.

2.1 Hydrodynamic model

The model equations are the nonlinear shallow equations:

$$\begin{aligned} &\frac{\partial \eta}{\partial t} + \nabla \cdot (H\mathbf{u}) = 0 \\ &\frac{\partial \mathbf{u}}{\partial t} + \mathbf{u} \cdot \nabla \mathbf{u} = -f\mathbf{e}_z \times \mathbf{u} - g\nabla\eta - \frac{g\|\mathbf{u}\|\mathbf{u}}{C^2 H} - C_S \frac{|\mathbf{u} \cdot \nabla H|}{H} \cdot \mathbf{u} + \frac{\boldsymbol{\tau}}{\rho H} + \frac{1}{H}\nabla \cdot [H\nu(\nabla \mathbf{u})] \end{aligned} \tag{2.1}$$

where $H = h + \eta$ is the water column depth, h is a reference depth level and η is the variation from this reference depth level, $\mathbf{u}$ is the horizontal depth-integrated velocity, f is the Coriolis factor, $\mathbf{e}_z$ is a unit vector pointing vertically upwards, $\boldsymbol{\tau}$ is the surface wind stress, g is the gravitational acceleration, ρ is the water density, ν is the horizontal viscosity, C is the Chezy bottom-stress coefficient and C_S is the numerical slope stress coefficient.

The bathymetry is found by extracting data from the ETOPO1 1 Arc-Minute Global Relief Model developed by the National Geophysical Data Center (NGDC) [Amante and Eakins, 2009] (see figure 2.1). In addition to this bathymetry, we also received more precise bathymetry measurement from Sam Purkis[2] on Great Bahama bank and Cay Sal Bank (CSB) (see figure 2.2). These two bathymetries are then merged in our model. However, as shallow water equations can only be solved for positive values of H, the minimum depth was set to $h = 3$ m in order to make sure the entire domain is under water at all time. However, we later got rid of this restriction using wetting-drying methods (see section 2.5).

The Chezy bottom-stress coefficient is defined as $H^{(1/6)}/n$, where n is the Manning coefficient. In this study ,the Manning coefficient is taken to be $n = 0.03$ m$^{-1/3}$s, which is pretty close

[1] **S**econd-generation **L**ouvain-la-Neuve **I**ce-Ocean **M**odel: `http://www.climate.be/slim`
[2] Department of Marine Geosciences, University of Miami - RSMAS

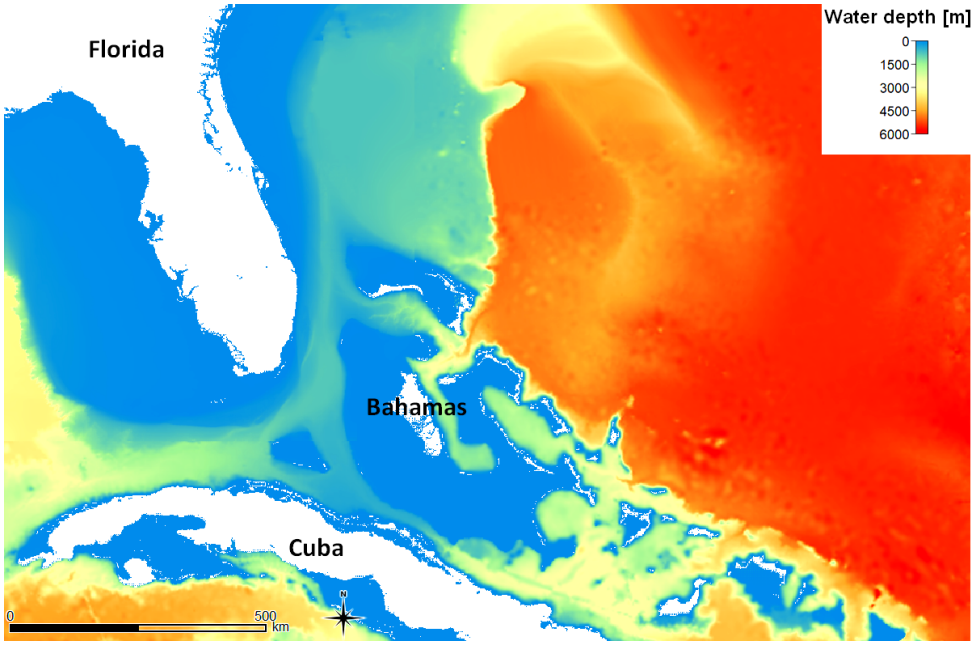

Fig. 2.1: Bathymetry used in our model

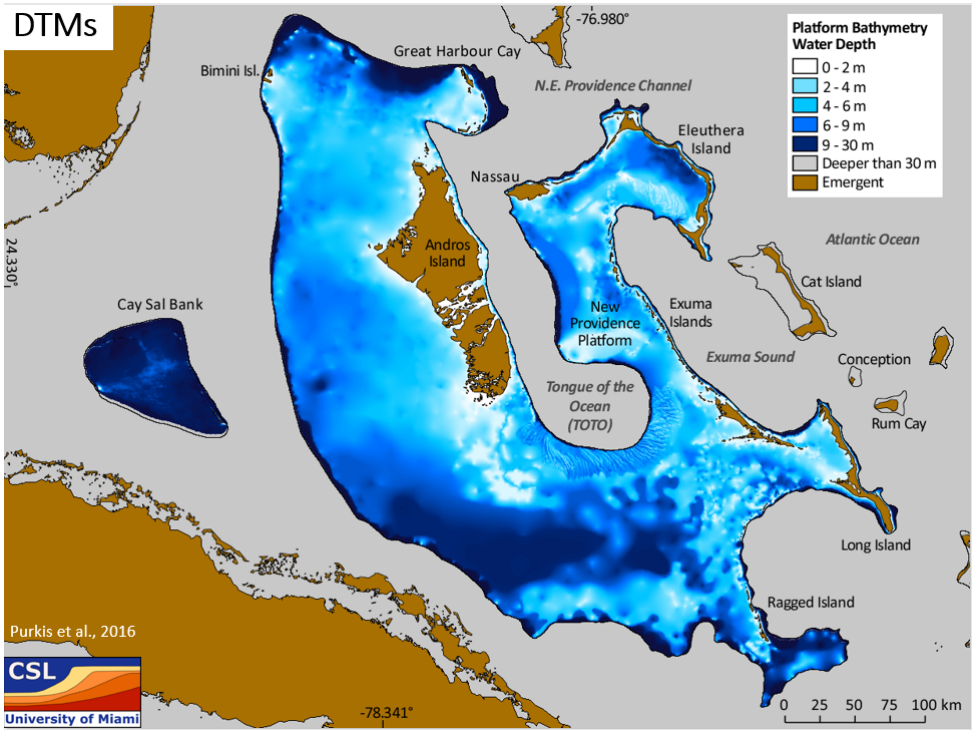

Fig. 2.2: Precise bathymetry measurements on Great Bahama Bank and Cay Sal Bank [Purkis et al., 2016]

to the value $n = 0.025$ m$^{-1/3}$s used in [De Brye et al., 2010] . This Chezy-Manning-Strickler friction term is combined with a slope-dependent friction term defined as in [Döös et al., 2004] on account of the important bathymetry gradient ∇H surrounding Great Bahama Bank. The numerical slope coefficient is chosen to be $C_S = 5$ in this study, which corresponds to the value used in [Frys, 2017] for the Florida Reef Tract.

The surface wind stress is computed as follows:

$$\boldsymbol{\tau} = \rho_{\text{air}} C_D \|\mathbf{u}_{10}\| \mathbf{u}_{10} \tag{2.2}$$

where ρ_{air} is the air density, C_D is the drag coefficient and $\mathbf{u}_{10}$ is the wind velocity [ms^{-1}] 10 meters above the sea surface [Cushman-Roisin and Beckers, 2011]. The wind speeds are extracted from Climate Forecast System (CFS) model of the National Center for Environmental Prediction (NCEP) [Saha et al., 2010, 2014]. The Smith and Banke parametrization is chosen for the drag coefficient C_D in order the take the impact of stronger winds on the sea surface into account [Smith and Banke, 1975]:

$$C_D = (\alpha + \beta \|\mathbf{u}_{10}\|) \cdot 10^{-3} \tag{2.3}$$

with $\alpha = 0.63$ and $\beta = 6.6 \cdot 10^{-2}$ m^{-1}s. This parametrization is applicable for wind speeds ranging from 3 to 21 ms^{-1} [Geernaert, 1987], which is within the order of magnitude of the winds observed on our study region.

Finally, Smagorinsky parametrization [Smagorinsky, 1963] is used for the viscosity ν in order to take unresolved turbulent features into account:

$$\nu = (\tilde{C}_S \Delta)^2 \sqrt{2\left(\frac{\partial u}{\partial x}\right)^2 + 2\left(\frac{\partial v}{\partial y}\right)^2 + \left(\frac{\partial u}{\partial y} + \frac{\partial v}{\partial x}\right)^2} \tag{2.4}$$

with Δ the local mesh element size, (x, y) the Cartesian coordinates of the horizontal plan, (u, v) the component of the depth integrated velocity $\mathbf{u}$ and the Smagorinsky coefficient $\tilde{C}_S = 0.1$ [Lambrechts et al., 2008].

2.2 Unstructured mesh

Using unstructured mesh allows us to use a large computational domain and keep boundaries away from the region of interest. A high resolution is then used in the regions we need to focus on while a coarser resolution is used in the rest of the domain. Doing so, one avoids unwanted spurious effects [Le Roux et al., 2005] in the neighborhood of the open boundaries. In our case, the resolution of a mesh element is influenced by two parameters: proximity of coastlines and water depth.

First, to take coastal physical features into account, we define a mesh size $\Delta_c(d)$ [m] depending on the distance to the nearest coastline d (in meters):

$$\Delta_c(d) = \begin{cases} 10^3 & \text{if } d \leq d_0 \\ 10^3 \dfrac{d_1 - d}{d_1 - d_0} + 10^4 \dfrac{d - d_0}{d_1 - d_0} & \text{if } d_0 \leq d \leq d_1 \\ 10^4 & \text{otherwise} \end{cases} \tag{2.5}$$

with $d_0 = 8 \cdot 10^3$ m and $d_1 = 5 \cdot 10^4$ m.

Furthermore, we want to have a high resolution on our study region, the GBB, which is characterized by a maximum water depth of about 10 m. We thus decide to have a mesh size of

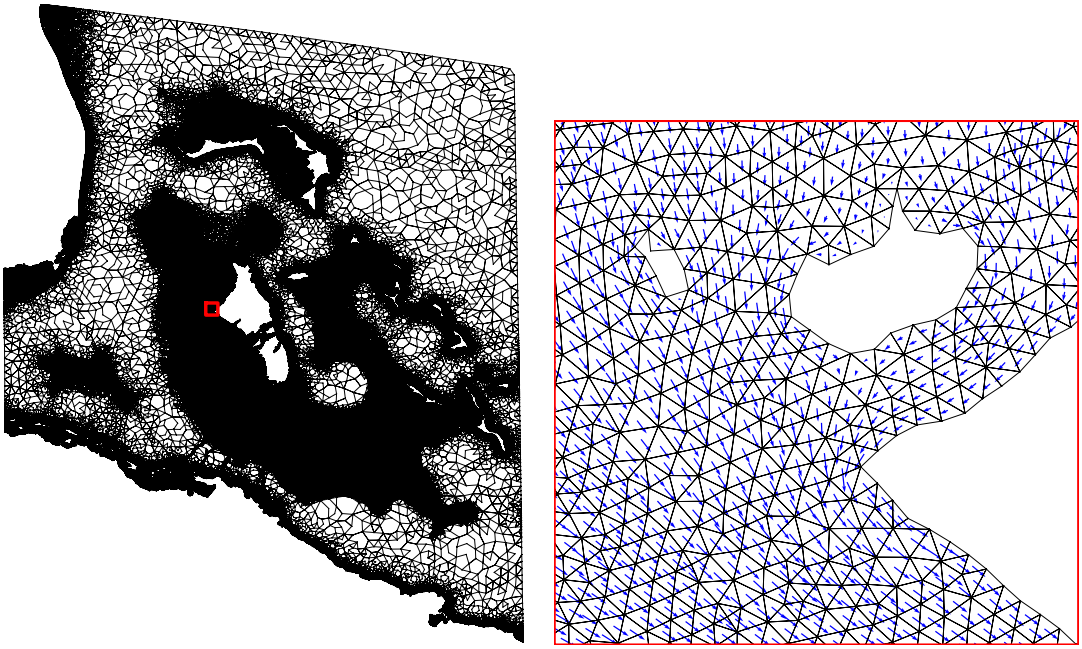

Fig. 2.3: On the left side: the mesh used in our study. On the right side: a zoom on the GBB (red box) in order to visualize the finest 670 m mesh resolution

about 1 km on a 10 meters deep region. We define thus the following water depth dependent mesh size:

$$\Delta_{wd}(h) = 300\sqrt{\min(1000, \max(5, h))} \tag{2.6}$$

The local mesh size Δ [m] is then computed by taking the minimum of Δ_c and Δ_{wd}. One then obtains the mesh of figure 2.3 with coarsest elements of about 22 km. Such a mesh has about $4.4 \cdot 10^5$ elements.

2.3 Model forcings

In order to obtain realistic hydrodynamics on the Bahama Banks, one must apply three external forcings on the model: winds, tides and large scale water circulation due to the Gulf Stream. To apply these forcings, three different datasets are used. Given that these datasets make use of regular grid, one needs to perform an interpolation on the unstructured grid of the mesh.

As said in section 2.1, wind speeds 10 meters above the see surface where extracted from NOAA databases and then integrated in equation 2.2. An example of the value of the wind forcing on the Great Bahama Bank is given in figure 2.4.

Tidal forcing is extracted from the OSU TOPEX/Poseidon Global Inverse Solution TPXO dataset [Egbert and Erofeeva, 2002], which gives the amplitude and phase of the main tidal components on a $1/4^\circ$ resolution global grid. These components can then be reconstructed into tidal elevation and velocity.
Currents data are taken from HYCOM[3]. The data provides 3D currents on a $1/12^\circ$ lon/lat grid interpolated on 40 z-levels. A depth-averaging of the velocities must thus be performed in order to use HYCOM data in our 2D model. HYCOM elevation and velocities summed with TPXO tidal elevation and velocities are imposed on the orange open boundaries of figure 2.6 in order to obtain the Gulf Stream along the Florida peninsula as well as water circulation on the

[3]HYCOM + NCODA Global $1/12^\circ$ Analysis (GLBu0.08) `https://hycom.org/data/glbu0pt08`

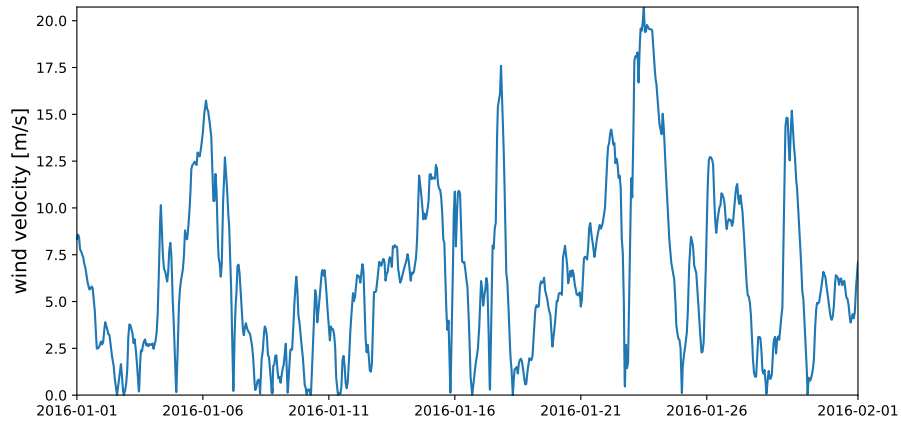

Fig. 2.4: Example of wind forcing on the Great Bahama Bank (green point on figure 2.6)

Atlantic Ocean on the east.
However, TPXO tidal velocities are not very accurate on shallow coastal regions. This resulted in too high velocities imposed in the vicinity of the coastlines of Cuba and in the Florida Keys on the open boundary of our domain with the Gulf of Mexico. To address this problem, we filtered the imposed velocities on the western open boundary of our domain with respect to bathymetry h using a coefficient $\alpha(h)$ defined as follows:

$$\alpha(h) = \begin{cases} 0 & \text{if } h < 10 \\ 1 & \text{if } h > 50 \\ 0.25 \cdot (0.10 \cdot h - 1) & \text{otherwise} \end{cases} \tag{2.7}$$

As said earlier, HYCOM is a 3D model, which makes it more efficient to reproduce physical processes in deep water (e.g. large-scale eddies) than a 2D model such as SLIM. Hence, in order to improve our results, a relaxation term is added to our hydrodynamic model in order to keep SLIM modeled velocities close to HYCOM ones where needed. This resulting global circulation forcing writes:

$$\mathbf{F}_{\text{gc}} = \gamma(\mathbf{u}_* - \mathbf{u}) \tag{2.8}$$

where $\mathbf{u}_*$ is the sum of HYCOM velocities with TPXO tidal velocities and $\gamma = \tau^{-1}$ is the inverse of the relaxation time. We parametrized γ as the sum of a term $\gamma_c(d)$ depending on the distance to the nearest coast and a term $\gamma_{wd}(h)$ depending on bathymetry h. These two terms are defined as follows

$$\gamma_c(d) = \begin{cases} 1 - 10^{-5} d & \text{if } d \leq 10^5 \\ 0 & \text{otherwise} \end{cases} \qquad \gamma_{sw}(h) = \begin{cases} 0 & \text{if } h < 50 \\ 10^{-7} H & \text{if } 50 \leq h \leq 300 \\ 3 \cdot 10^{-5} & \text{otherwise} \end{cases} \tag{2.9}$$

The value of $\gamma(d,h) = \gamma_c(d) + \gamma_{sw}(h)$ over the simulation domain is given on figure 2.5.

2.4 Validation of the hydrodynamics

Validation of our model was pretty difficult due to the poor amount of data available on the Great Bahama Bank. The only data we found were sea surface elevation measurements from a tide gauge located 100 m away from Freeport's harbor (cf figure 2.6), which is pretty far away from the zone where whitings occur. Furthermore, this only gave us measurements of the sea surface elevation at that point and no information about currents velocity. The comparison of SLIM output with this validation data for January 2016 is shown in figure 2.7.

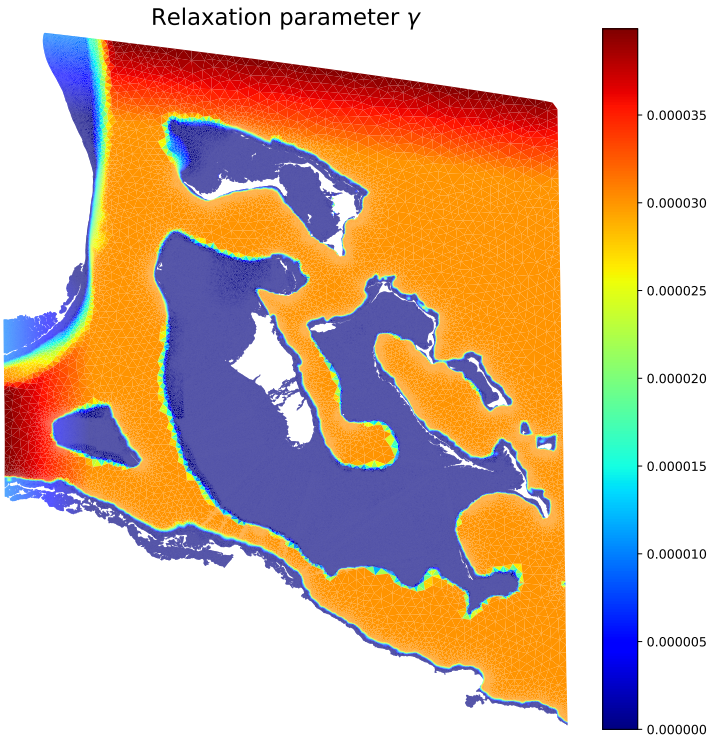

Fig. 2.5: Value of the relaxation parameter γ over the simulation domain

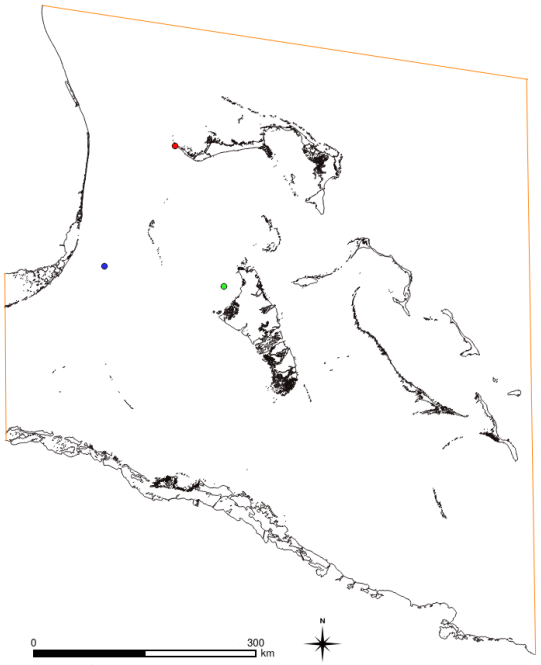

Fig. 2.6: Location of the validation points on Little Bahama Bank (red), Great Bahama Bank (green) and Florida Straits (blue) and the boundaries of the hydrodynamic model. Closed boundaries (coasts) are represented in black, open boundaries in orange.

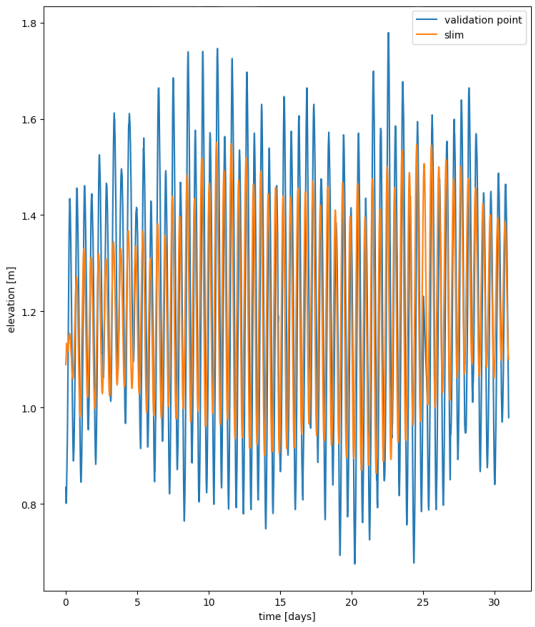

Fig. 2.7: Comparison of SLIM sea surface elevation and the measurements at the validation point on Little Bahama Bank (red point on figure 2.6)

One can then notice that SLIM elevation's amplitude is smaller than the one measured at the validation point. Yet, as this point was not the most consistent to assess our results on the Great Bahama Bank and although our results did not perfectly match the validation data, the difference seemed acceptable to us since a good match with other validation tests was obtained (see below). Moreover, one can observe a slight phase difference between the data and our model, which is due to a bad parametrization of the friction terms. This issue was not addressed due to a lack of time.

Another way to assess SLIM results is to confront them with the ones of another model. We thus compared the results of SLIM with HYCOM elevation and velocity combined with TPXO tidal elevation and velocity in the region of the Gulf Stream, where HYCOM is supposed to be accurate. One might argue that this validation test is a bit doubtful since we impose our model to stick to HYCOM + TPXO through the relaxation coefficient γ. However, in the absence of other validation data, this allowed us to evaluate the behavior of our model on the Florida Straits. The obtained curves are given in figure 2.8.

As expected from the forcings, the results of our model were fairly close to the ones of HYCOM and TPXO. Assuming accuracy of HYCOM, one might thus expect our model to predict reliable values of currents on Florida Straits, and therefore reliable value of current reaching the margin of the Great Bahama Bank. Still, this gives us no insurance on the accuracy of the currents modeled on the platform.

That being said, one major weakness of our model remains that it cannot handle dry zones. To avoid this problem, we therefore modified our bathymetry in order to have a minimal water-depth of 3m all over the domain. This approach had two drawbacks. First of all, as our region of interest, the Great Bahamas Bank, is mostly shallower than 10m, discarding all zones less than 3m deep is a substantial modification of the topology of the platform that might result is some inaccuracies of our model. Secondly, one has no guarantee that no element of our domain will encounter tidal oscillations larger than 3m, especially for long simulations of one year. Hence, despite the applied water-depth modification, our model was unable to converge at the 6708th simulated hour (beginning of October 2016) due to a dry zone on Little

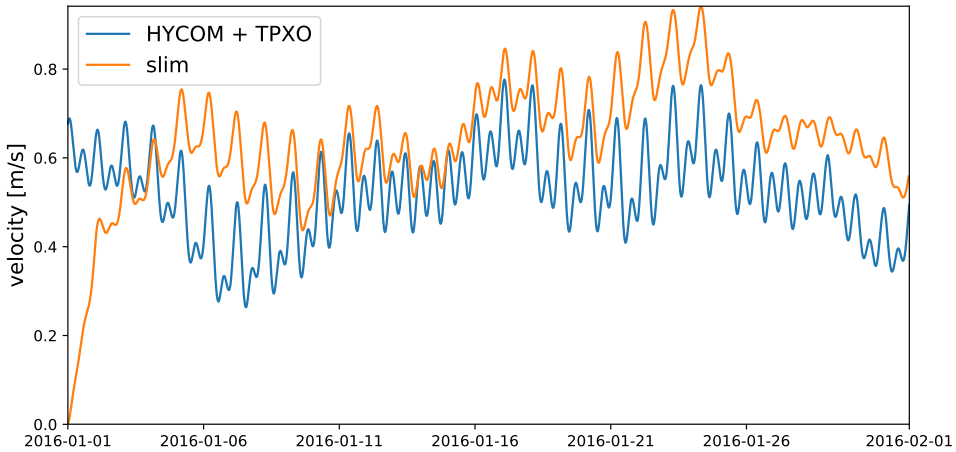

Fig. 2.8: Comparison of SLIM and HYCOM results in the region of the Gulf Stream (blue point on figure 2.6)

Bahama Bank, were the bathymetry of our model was the most dubious. In order to overcome this difficulty, we used wetting-drying (WD) methods.

2.5 Wetting-drying

Most of the world's coastal seas are connected to embayments, estuaries and lagoons. When approaching the coasts of these regions, tidal signal tends to amplify which, combined with the fact that these zones usually feature gradually sloping bathymetry, causes the extent of areas subject to alternating wetting and drying (or tidal-flats) during the tidal cycle to be potentially as large as the permanently-submerged areas. Moreover, tidal flats play a very important role in the ecosystems of such coastal areas. The ability to accurately simulate the wetting and drying process is thus a key-feature in coastal eco-hydrodynamic modeling [Gourgue et al., 2009].

Wetting-drying methods can be classified into two main categories: the deformed mesh or Lagrangian methods and the fixed mesh or Eulerian methods. These first methods, although yielding the most appropriate description of the wetting-drying process, are faced with several difficulties. First, a parametrization must be built in order to move the domain boundary as a function of the flow in boundary elements [Marchandise and Remacle, 2006; Sobey, 2009]. Secondly, advanced algorithms must be designed in order to maintain a good mesh quality in long simulations. And finally, the greatest drawback is the high computational coast of deforming the mesh. This is mainly why deforming mesh wetting-drying has rarely been applied on real-world problems [Yuan et al., 2008; Zheng et al., 2003; Zijlema and Stelling, 2008].

Most of the available WD methods have therefore been developed for fixed meshes. The Eulerian methods can be subdivided into two main approaches: the flux-limiting methods, that only modify the discrete algebraic form of the hydrodynamics equations and the so-called modified equation methods, for which the original continuous form of the original partial differential equations is modified.

In the flux-limiting methods, either nodes or entire elements are deactivated when becoming dry, the dry state being usually detected via some special water depth based criteria. In the first attempts of flux-limiting methods, entire elements were either tagged as "dry" or "wet", dry elements elements being excluded from the computational domain. This implied two main drawbacks. First, the WD interface can only be located at element edges which have

an impact on the boundary layer behavior [Bates and Hervouet, 1999]. Secondly, sudden inclusion/exclusion of elements may break mass end momentum conservation or generate numerical instability [Van't Hof and Vollebregt, 2005].
To overcome these problems, the most popular method is to leave a thin water layer in the dry areas to ensure a positive water depth and maintain a continuum across the interface [Bunya et al., 2009; Nikolos and Delis, 2009]. The transition elements are then defined as elements for which some nodes, but not all of them, are dry. Dry being defined as having a water level under a certain threshold value. However, coexistence of dry and wet nodes on a same element may then generate spurious water slope resulting in artificial pressure gradients that drive water down [Heniche et al., 2000], which causes wet nodes to dry out if not treated properly. Treatment of the transition is thus the main difficulty of thin layer methods and requires explicit detection of dry elements, so that WD front can propagate only by one node each time step. However, time step is generally bounded to ensure positive water depth or numerical stability [Casulli, 2009]. This results in a significant growth of the computation cost, especially for large scale simulations embodying both deep and shallow areas [Stelling and Duinmeijer, 2003].

The first method among the modified equation approach is the artificial porosity method [Heniche et al., 2000; Stelling and Duinmeijer, 2003]. In this method, the seabed is assumed to be porous and non-zero water fluxes are then allowed for negative depths, generating a so-called porous layer [Ip et al., 1998; Nielsen and Apelt, 2003]. The main advantage of these methods is that spurious surface slopes disappear as free surface falls under bed into the porous media during drying phase. On the other hand, "virtual" water is generated as depth attains negative values, even though mass conservative formulations are known to exist [Defina, 2000]. Finally, the key advantage of these methods comes from the fact that transitions between wet and dry is smooth and modifications are expressed in the primitive equations. Therefore, Jacobian of the system can be computed, which permits the use of semi-implicit or implicit [Heniche et al., 2000; Ip et al., 1998] time integration and significantly reduces computational cost.
The second approach among the modified equation methods is the damping or kinematic method. This method is exploiting the fact that wetting-drying processes are essentially dominated by pressure gradient and bottom friction to simplify the equations [Ip et al., 1998; Burchard et al., 2004], leading to the so-called diffusive wave approximation of the shallow water equations [Alonso et al., 2008; Santillana and Dawson, 2010]. Nonetheless, this approach is not applicable to coastal waters in most cases.

The wetting-drying method used in SLIM is an alternative "negative-depth" implicit WD formulation based on the idea that the bed is allowed to move in time as water elevation drops [Kärnä et al., 2011]. Such method does not need the introduction of the porosity concept, yields simpler implementation and has only one unknown parameter whose value can be estimated in a fairly reliable way. Even though the notion of moving bathymetry may seem unusual, similar modifications have been locally applied in certain WD methods [Burchard et al., 2004; Nikolos and Delis, 2009; Castro et al., 2005] in order to avoid spurious pressure forces at the WD interface.
To ensure positive water depth, a smooth continuously derivable function f is introduced and bathymetry is redefined as $\tilde{h}(\eta, h) = h + f(\eta + h)$. The function f is chosen so that the redefined total depth $\tilde{H} = \eta + \tilde{h}$ remains positive. The sea surface elevation then writes $\tilde{\eta} = \tilde{H} - \tilde{h} = \eta + f$. Equations 2.10 are then modified in such a way that $\tilde{H}$ is being conserved:

$$\begin{aligned} &\frac{\partial \eta}{\partial t} + \frac{\partial \tilde{h}}{\partial t} + \nabla \cdot (\tilde{H}\mathbf{u}) = 0 \\ &\frac{\partial \mathbf{u}}{\partial t} + \mathbf{u} \cdot \nabla \mathbf{u} = -f\mathbf{e}_z \times \mathbf{u} - g\nabla\eta - \frac{g\|\mathbf{u}\|\mathbf{u}}{C^2\tilde{H}} - C_S\frac{|\mathbf{u} \cdot \nabla\tilde{H}|}{\tilde{H}} \cdot \mathbf{u} + \frac{\boldsymbol{\tau}}{\rho\tilde{H}} + \frac{1}{\tilde{H}}\nabla \cdot \left[\tilde{H}\nu(\nabla\mathbf{u})\right] \end{aligned} \tag{2.10}$$

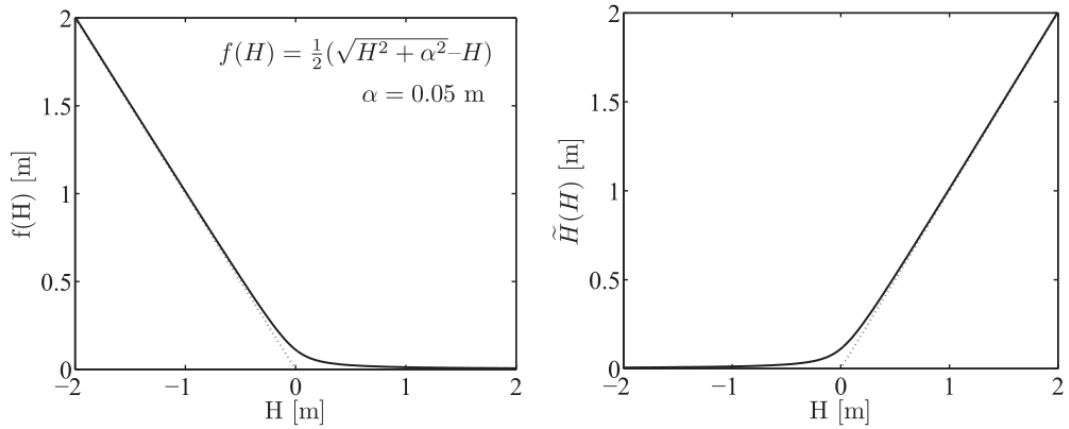

(a) Function $f(H)$ (b) Modified total depth $\tilde{H}$

Fig. 2.9: Function defining moving bathymetry [Kärnä et al., 2011]

The continuity can be further developed using $\frac{\partial \tilde{h}}{\partial t} = f'(H)\frac{\partial \eta}{\partial t}$:

$$(1 + f'(H))\frac{\partial \eta}{\partial t} + \nabla \cdot (\tilde{H}\mathbf{u}) = A(H)\frac{\partial \eta}{\partial t} + \nabla \cdot (\tilde{H}\mathbf{u}) = 0 \tag{2.11}$$

where $0 < A < 1$ is a smooth indicator that ranges from dry ($A \approx 1$) to wet ($A \approx 0$) and is interpreted as the proportion of total element area that is penetrable by water. This is the smoothness of A that prevents spurious oscillations and permits implicit time marching.

Regarding the choice of f, this function should respect the following properties:

1. $\tilde{H} = H + f(H) > 0$ for all H
2. $f \approx 0$ for $H \gg 1$
3. f must be continuously derivable

The second property imposes that modification of the bathymetry is restricted to shallow areas while the third one ensures convergence of Newton iterations. These 3 conditions are fulfilled by:

$$f(H) = \frac{1}{2}\left(\sqrt{H^2 + \alpha^2} - H\right) \tag{2.12}$$

The α parameter (dimension is meters) of the function affects the width of the transition between wet ($A(H) \leq 1$, $f(H) \approx 0$) and dry ($A(H) \leq 0$) areas, as shown in figure 2.9. To ensure robustness, WD interface should be smooth, implying that the transition zone should cover more than one element. Estimating the variation in bathymetry within one element by:

$$\epsilon := L_x|\nabla H| \tag{2.13}$$

where L_x is the horizontal length scale, one can assume $\alpha \approx \epsilon$ to be used as an heuristic for increasingly sloping domains. However, some more restrictive constraints may be applied for numerical stability but these are more difficult to estimate a priori.

To overcome the convergence issue of our model, we used the wetting-drying version of the 2D barotropic module of SLIM with $\alpha = 0.5\ m$. However, the bathymetry used with this module was cropped in order to have $h \geq 1\ m$ on the whole domain. This choice was made in order to increase the convergence rate of the time integration of the equations.

2.6 Limitations

The main drawback of our model lies in its strength and comes from the fact that it is a 2D model. What is won in computational cost is lost in physical accuracy . Indeed, upwelling events and baroclinic dynamics are poorly handled by our model. Moreover, since the aim of this work is investigating whitings formation, bottom sediment resuspension must be studied. As this phenomenon is depth dependent, our 2D model might not be the the best suited tool despite its high resolution.
Furthermore, although our model reproduces global water circulation outside the banks in a fairly reliable way thanks to our relaxation term, it is pretty complicated to evaluate its behavior on Great Bahama Bank due to lack of measurements. Results of the model on the platform can only be assessed a posteriori, after they have been used in more advanced studies.

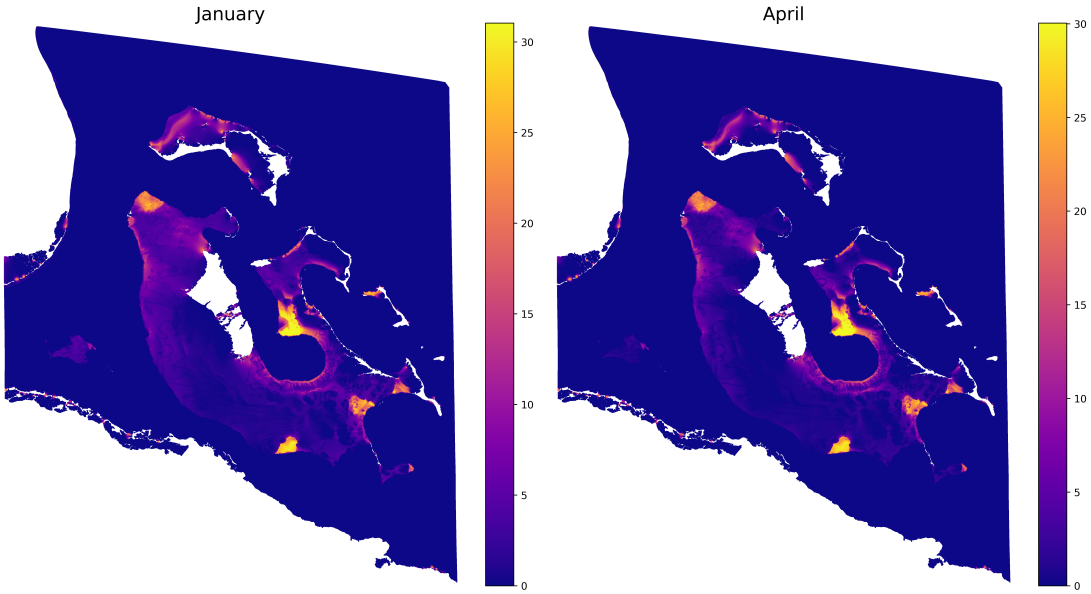

Fig. 3.1: Cumulated time over 0.2 ms^{-1} on the GBB for January and April, time units on the colorbar are days

3 Designing indicators to study whitings

After validation of the hydrodynamics, we can now use the output of our simulations to design indicators to highlight physical phenomena that might intervene in the process of whitings formation and then compare their predictions with observations. As whitings are suspected to be due to both a resuspension and a precipitation mechanism, our indicators will be focused on currents velocity on the one hand to study bottom sediments resuspension and on water mixing on the other hand in order to study changes of water chemistry. In this section, we will detail the different indicators we came up with and the information they brought us.

3.1 Bottom sediment resuspension indicators: threshold and mean velocity

The first mechanism we tried to investigate through indicator designing is bottom-sediment resuspension. According to [Boss and Neumann, 1993] and [Neumann et al., 1970], currents velocities of 0.2 ms^{-1} are sufficient to erode seabed for natural carbonate sand such as in the Bahamas. As first indicator, we hence decided to compute for each month the cumulated time during which the velocity was larger or equal to 0.2 ms^{-1} on the GBB. To do so, we defined for each node k of coordinates $\mathbf{x}_k$ ($k = 0, 1, \cdots, N-1$) one indicator value I_k first set to zero. Then, at every time step t_i ($i = 0, 1, \cdots, N_t - 1$), we performed:

$$\begin{cases} I_k \leftarrow I_k + \Delta t & \text{if } \|\mathbf{u}(\mathbf{x}_k, t_i)\| \geq 0.2 ms^{-1} \\ I_k \text{ unchanged} & \text{otherwise} \end{cases} \tag{3.1}$$

for every node of the mesh, were Δt is the time step and $\mathbf{u}(\mathbf{x}_k, t_i)$ is the horizontal depth-integrated velocity predicted by SLIM at point $\mathbf{x}_k$ at time t_i. The points for which the indicator I_k would take the highest value on the Bank would then be considered as the zones where whitings are most likely to occur. An example of the figures we obtained with this first indicator are given in figure 3.1

One can first notice that this indicator seems to be in pretty good accordance with observation. Indeed, from a spatial perspective, the lighter region on the west of Andros Island corresponds

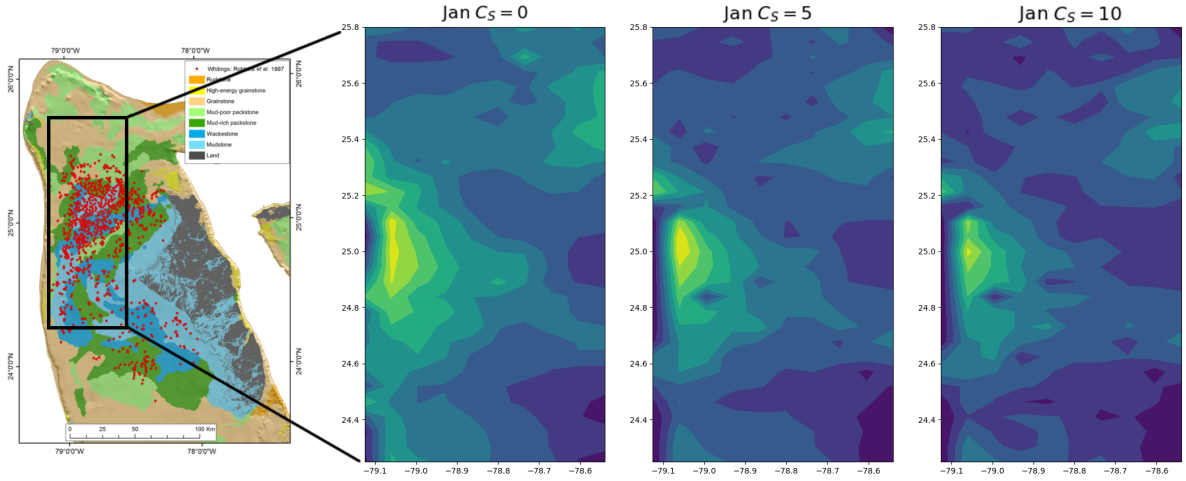

Fig. 3.2: Comparison of the threshold velocity indicator in January 2016 for different values of the gradient-dependent slope coefficient C_S. Yellow regions correspond to high values of the operator while dark blue regions correspond to small values

more or less to the zone of high whitings occurrence on figure 1.3. However, from a temporal perspective, there is no strong difference in the value of our indicator between January and April, which is the month with the most observed whitings according to [Robbins et al., 1997].

3.1.1 Impact of the slope-dependent friction parameter

Most of the parameters used in our model are given pretty standard values based on physics and previous works. The slope-dependent friction coefficient C_S on the other hand is a purely numerical and nondimensional parameter whose value is more case-dependent. We thus wanted to study the influence of this parameter on our threshold velocity indicator. For this study, we only considered a rectangle surrounding the region where most of whitings are observed on figure 1.3. The obtained figures are shown in figure 3.2

As one could expect, increasing the friction on the embankment surrounding the plateau of the GBB decreases the velocity on the bank, which causes a reduction of the regions with high indicator values in the study zone. However, this does not have an important impact on the spatial distribution of regions with high and low values of the indicator. In the absence of any "true" physical criterion to favor one particular value of C_S based on this study, we decided to keep the parametrization of [Frys, 2017], in which $C_S = 5$ was used on the Florida Keys. We assumed this region to be similar to the GBB.

3.1.2 Mean and standard deviation of the velocity

In addition to this first velocity-based indicator, we also computed the mean and standard deviation of the norm of the velocity on the GBB for each month.

$$\begin{aligned} u_{mean}(\mathbf{x_k}) &= \frac{1}{N_t} \sum_{i=0}^{N_t-1} \|\mathbf{u}(\mathbf{x}_k, t_i)\| \\ u_{std}(\mathbf{x}_k) &= \sqrt{\frac{1}{N_t - 1} \sum_{i=0}^{N_t-1} (\|\mathbf{u}(\mathbf{x}_k, t_i)\| - u_{mean}(\mathbf{x_k}))^2} \end{aligned} \tag{3.2}$$

Such mean velocities are mostly tidally driven. The obtained figures are given in figure 4.2 and 4.3.In addition to these indicators, we also computed the monthly mean northward and eastward components of the velocity field in order to obtain additional information on the long-term water motions without high-frequency fluctuations originating from tidal variations. Using these mean components, one can then represent mean velocity field as in figure 4.5. Such currents are forced by winds alone.

3.2 Water chemistry indicators

In order to have whitings and thus aragonite precipitation, bank-top water must be sufficiently saturated with respect to aragonite. Since saturation state of platform-top waters is lower than the one of off-platform waters, we investigated water exchanges across the margin of the bank using two indicators: a Lagrangian particle tracker and the computation of a mean volume flow rate trough the 30m isobath, which defines the boundary of the bank.

Furthermore, most of the whitings formation mechanisms introduced in section 1.3 are amplified during warmer months of the summer: Ω and cyanobacteria photosynthetic rate increase [Jiang et al., 2015]. However, in practice, more whitings are observed during winter months, which seems to contradict thermodynamic and kinetic laws. A way to explain this higher occurrence frequency during winter might be through interaction between colder bank waters and warmer waters from the Florida Straits, which would permit the appearance of localized zones of relatively increased saturation state. Warming of the bank top waters would then release some of the dissolved CO_2, instantaneously increasing saturation state.

Finally, bank water on the GBB are isotopically enriched in ^{13}C, which has been attributed to high productivity rate. However, such an enrichment is only possible if water has a long residence time. This is why we computed the water age on the bank as last indicator.

3.2.1 Tracking of water mixing

In order to get an insight on the monthly mixing of deep and shallow waters, we tracked the dispersal of two types of particles on our study domain using the same Lagrangian particle tracker as in [Thomas, 2015] and [Frys, 2017]. This particle tracker uses a random walk formulation [Dimou and Adams, 1993; Spagnol et al., 2002] of an advection-diffusion equation and writes:

$$\begin{aligned} \mathbf{x}_{n+1} &= \mathbf{x}_n + \mathbf{v}_n \Delta t + \mathbf{R}_n \sqrt{\frac{2K\Delta t}{r}} \\ \mathbf{v}_n &= \left(\mathbf{u} + \frac{K}{H} \nabla H + \nabla K \right) \Big|_{\mathbf{x}_n} \end{aligned} \tag{3.3}$$

where $\mathbf{x}_n$ and $\mathbf{v}_n$ are the particles position and velocity at time iteration n, Δt is the time difference between iterations, K is the horizontal diffusivity coefficient, $\mathbf{u} = \mathbf{u}(\mathbf{x}, t)$ is the instantaneous depth-averaged horizontal water velocity modeled by SLIM, H is the water column depth and $\mathbf{R}_n$ is a two-dimensional vector of random numbers with zero mean and a variance of $r = \langle R^2 \rangle$. The time step $\Delta t = 900s$ was used in order to bound the distance traveled by a particle in a single time step. Moreover, the horizontal diffusivity coefficient was calculated using the parametrization presented in [De Brye et al., 2010], which makes use of the formula of Okubo [Okubo, 1971] to implement a dependence on local element size of the mesh as :

$$K = \alpha \Delta^{1.15} \tag{3.4}$$

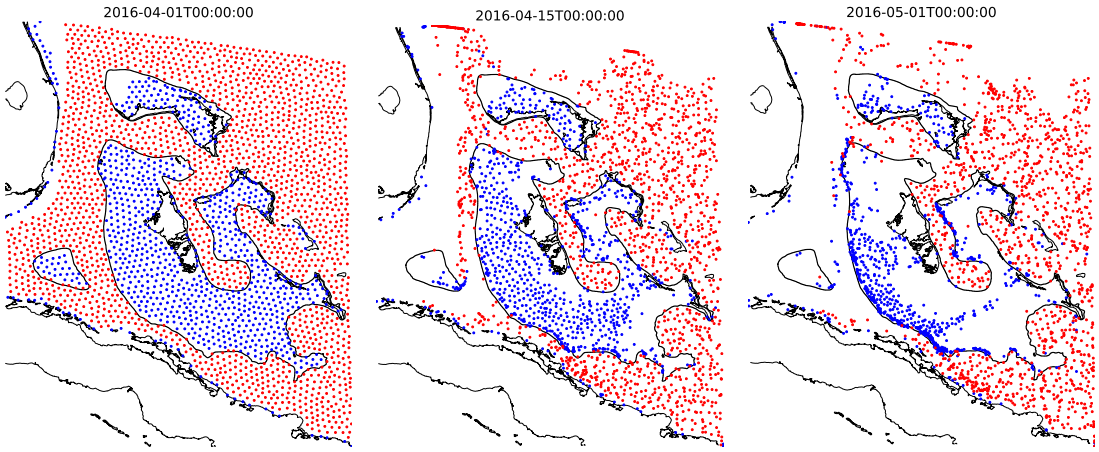

Fig. 3.3: Dispersal of deep water (red) and shallow water (blue) particles during April 2016 using basic shallow water equations

where Δ is the local mesh size and $\alpha = 0.00020551 m^{0.85} s^{-1}$. Dependence on local mesh size is of great importance since larger elements have a greater range of unresolved water motions than smaller ones. Okubo formula is one of the simplest implementation of this dependence and has been used in numerous studies (e.g. [Lambrechts et al., 2008] [de Brauwere et al., 2011], [Andutta et al., 2011] and [Van et al., 2016]).

This Lagrangian model was implemented as an additional module of SLIM and is run offline from the core hydrodynamic model. In other words, it reads sea surface elevation and velocity fields previously generated by the model as inputs and then use them to calculate the advection velocity of every particle. The outputs of SLIM were recorded every hour to allow tidal constituents to be accurately captured.

At the beginning of each month, particles were seeded following the nodes of a coarse complementary mesh of the study domain with a constant resolution of 10 km. A first type of particles (red on figure 3.3) were seeded on nodes located in deep regions ($\geq$ 200 m deep) while a second type of particles (blue on figure 3.3) were seeded on nodes located in shallow regions ($\leq$ 30 m deep). No particles were seeded on nodes located in the region that was between 30 and 200 meters deep. Tracking these particles during the month using equations 3.3 gives figure 3.3.

This indicator is quite imperfect since it does not actually measures water displacement but indirectly shows its effects though particles drifts. Moreover, we only have one seeding period at the beginning of the month. Therefore, once particles have been drifted away from their initial position, they are not replaced by new ones, which causes the appearance of "white" empty regions on the maps of figure 3.3. One has thus no information on the "new" water entering the system during the month.

Nevertheless, despite its weaknesses, this indicator gives a glimpse of water circulation and allows to build some intuition about how deep and shallow water stir together. For instance, one can see that the Gulf Stream has a huge impact on water circulation. Most of the particles are dragged up north due to its action and very few deep water seems to drift through the western boundary of the GBB. Moreover, as informal validation, the displacement of the blue particles from the Cay Sal Bank matches observed mud displacement due to currents after hurricanes.

3.2.2 Mean volume flow rate through the 30m isobath

Another way of tracking water exchanges between the bank and its surrounding is by computing water volume flow rate through the 30m isobath. The 30 m isobath, defining the outline of the Great Bahama Bank, was described by points of coordinates (x_k, y_k) stored in a shapefile. The isobath was then obtained by drawing the consecutive segments defined by the points (x_k, y_k) and (x_{k+1}, y_{k+1}). The monthly mean seaward component of the velocity was then computed on each of these segments as follows:

$$u_k^*(x_k^*, y_k^*) = \frac{1}{N_t} \sum_{i=0}^{N_t-1} \left(u(x_k^*, y_k^*, t_i) n_{k,x} + v(x_k^*, y_k^*, t_i) n_{k,y} \right) \tag{3.5}$$

where $x_k^* = \frac{x_{k+1}+x_k}{2}$ and $y_k^* = \frac{y_{k+1}+y_k}{2}$ are the coordinates of the middle point of the segment, $u(x_k^*, y_k^*, t_i)$ and $v(x_k^*, y_k^*, t_i)$ are respectively the eastward and northward components of the horizontal depth-integrated velocity computed by SLIM evaluated at time t_i ($i = 0, 1, \cdots, N_t - 1$) at (x_k^*, y_k^*) and $n_{k,x}$ and $n_{k,y}$ are the eastward and northward components of the seaward normal unit vector of segment k, defined as follows:

$$\begin{aligned} n_{k,x} &= \frac{(y_k - y_{k+1})}{\sqrt{(x_{k+1} - x_k)^2 + (y_{k+1} - y_k)^2}} \\ n_{k,y} &= \frac{(x_{k+1} - x_k)}{\sqrt{(x_{k+1} - x_k)^2 + (y_{k+1} - y_k)^2}} \end{aligned} \tag{3.6}$$

Mean volume flow rate through 10 km long portions of the platform margin were then obtain via surface integration of these mean seaward components of the velocity a follows:

$$Q_j = \sum_{k=k_j}^{k_{j+1}} 30 \cdot l_k \cdot u_k^* \tag{3.7}$$

where 30 is the 30m water depth on the isobath, l_k is the length of segment k and were k_j and k_{j+1} are defined such that $\sum_{k=k_j}^{k_{j+1}} l_k = 10$ km. Seaward ($u_k > 0$) and platformward ($u_k < 0$) fluxes were computed separately and put on the same figures (see figure 4.7) in order to see how they balance each other on a given 10km long portion of the margin. This allows us to make the difference between sections of the bank margin in which we have alternation of seaward and platformward fluxes, and portions for which fluxes were weak.

3.2.3 Water age

Finally, the last indicator we developed is a map of the water age on the Great Bahama Bank, i.e. the time elapsed since the water entered the GBB. Such map would update and expand the one derived by [Broecker and Takahashi, 1966] via chemical analysis. This paper predicts that the waters in the vicinity of Andros Island have a residence time of 200 days, whereas those located closer to the platform margin have times of 10 days only (see figure 3.4). In order to numerically compute the water age on the plateau, we worked in the framework of the Constituent-oriented Age and Residence time Theory (CART) [Delhez et al., 2011], which allows the estimation of water residence time and age in an Eulerian scheme by solving depth-integrated advection-diffusion-reaction equations. This is performed by defining the age of water of a given water type by the mean of two variables: the concentration $c_i(\mathbf{x}, t)$ and age concentration $\alpha_i(\mathbf{x}, t)$ of water type i. One then solves an advection-diffusion equation for c_i to simulate the propagation of water type i in the domain while an advection-diffusion-reaction

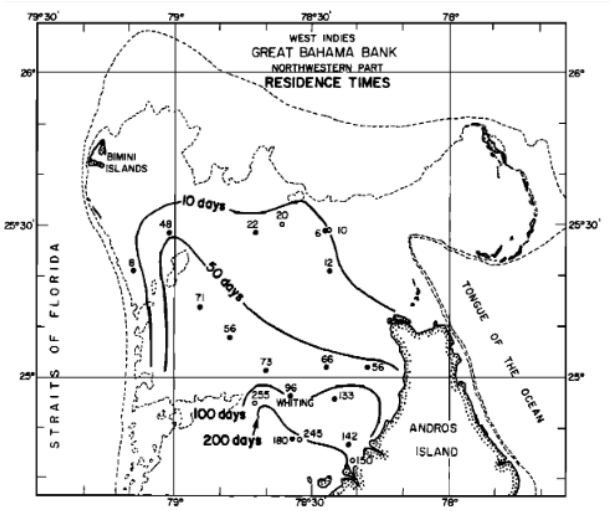

Fig. 3.4: Map with residence time contour [Broecker and Takahashi, 1966]

equation is solved for α_i, the addition of a constant reaction term accounting for the fact that age increases at a constant rate with time. The age a_i of a given given water type is then computed as follows:

$$a_i = \frac{\alpha_i}{c_i} \tag{3.8}$$

However in our case, only one type of water is considered. Therefore $a = \alpha$ and the problem simplifies to the resolution of one single advection-diffusion-equation for the age of water.

Let us define our domain of interest, the Great Bahama Bank, as Ω and its boundary $\partial\Omega = \Gamma_c \cup \Gamma_i$, where Γ_c are the coastlines and Γ_i is the 30m isobath. The equation we solved on Ω is similar to the one used in [de Brye et al., 2013] and writes:

$$\frac{\partial}{\partial t}(Ha) + \underbrace{\nabla_h(H\mathbf{u}a)}_{advection} = \underbrace{\nabla_h \cdot (H\mu_h \nabla_h a)}_{diffusion} + \underbrace{H}_{reaction} \tag{3.9}$$

where a is the water age, H is the water depth, $\mathbf{u}$ is the depth-averaged horizontal velocity and μ_h is the diffusivity coefficient. 3.9 is combined with the boundary condition $a(\mathbf{x}, t) = 0$ $\forall \mathbf{x} \in \Gamma_i$ to impose a zeros age to a water parcel when it enters or leaves the GBB. The reaction term is set to H to impose a unit growth rate of the age with time while the horizontal velocity governing the advection term is the one predicted by SLIM. Here again, the horizontal diffusivity coefficient was computed using the formula of Okubo.

4 Basic shallow water equations: results

We first performed simulations using the "classic" 2D shallow waters equations. As said above, we did not succeed to simulate the entire year with this first attempt, as one node of our mesh got dry on Little Bahama Bank. However, this first simulation gave us valuable insight on hydrodynamics on the Great Bahama Bank. These first results are given and analyzed in the following sections.

4.1 Resuspension indicators

As said in section 3.1, no strong variation of the value of the threshold velocity indicator is observed through months of simulation on figure 4.1. Regions which are the most exposed to current velocity larger than 0.2 ms^{-1} seem to remain the same all year long. One may also notice that there is a region with an indicator value relatively higher than the one of its surrounding located on the western margin of the GBB, facing the northern half of Andros Island. This area corresponds to the southern part of the zone where whitings are observed (black shape on figure 4.2).

Moreover, some slight fluctuations of the indicator value seem to occur south to the Tongue of the Ocean and northwest to Andros Island. If the first fluctuations, taking place outside the region where whitings are observed, are not of great interest, the second are more intriguing. Indeed, velocities larger than 20 cms^{-1} seem to occur at a higher frequency northwest to Andros Island from January through March, which are winter months. These increase of the indicator value during winter months might then be linked to increased whitings frequency during winter months.

No important fluctuations of monthly means and standard deviations of the norm of the velocity can be observed on figures 4.2 and 4.3) either. Zones with relatively high threshold velocity indicator values are also zone with high mean velocity norm figures, which confirms the existence of a relatively high velocity zone in the vicinity of the whitings hot spot. Monthly standard deviation of the velocity norm seems to mostly fluctuate south to the Tongue of the Ocean and remain pretty constant west and northwest to Andros Island. In this latter region, zones with large standard deviation of the velocity seem to correspond to regions with large mean velocity norms. Regarding bottom sediment resuspension, this is pretty interesting since some of the mechanisms for bottom-sediment resuspension introduced in section 3.1 (e.g. tidal burst) imply important variations of currents velocity. Finally, one can notice that mean velocity norm northwest to Andros Island is slightly higher during winter than during summer (see figure 4.4), which might be relevant to explain that whitings are 70% more numerous in winter. However this result is to be taken with a pinch of salt since some months are missing.

In conclusion, even though our velocity-based indicators suggest that bottom-sediment resuspension might take place in the region where whitings occur due to a relatively high velocity zone on the western margin of the Bank, these indicators do not strongly favor a month over another, except for a slight increase of mean velocity norm northwest to Andros Islands during winter month. Therefore, based on these indicator, resuspension does not seem to be the driving mechanism of whitings formation. Water chemistry will thus be investigated using our other indicators.

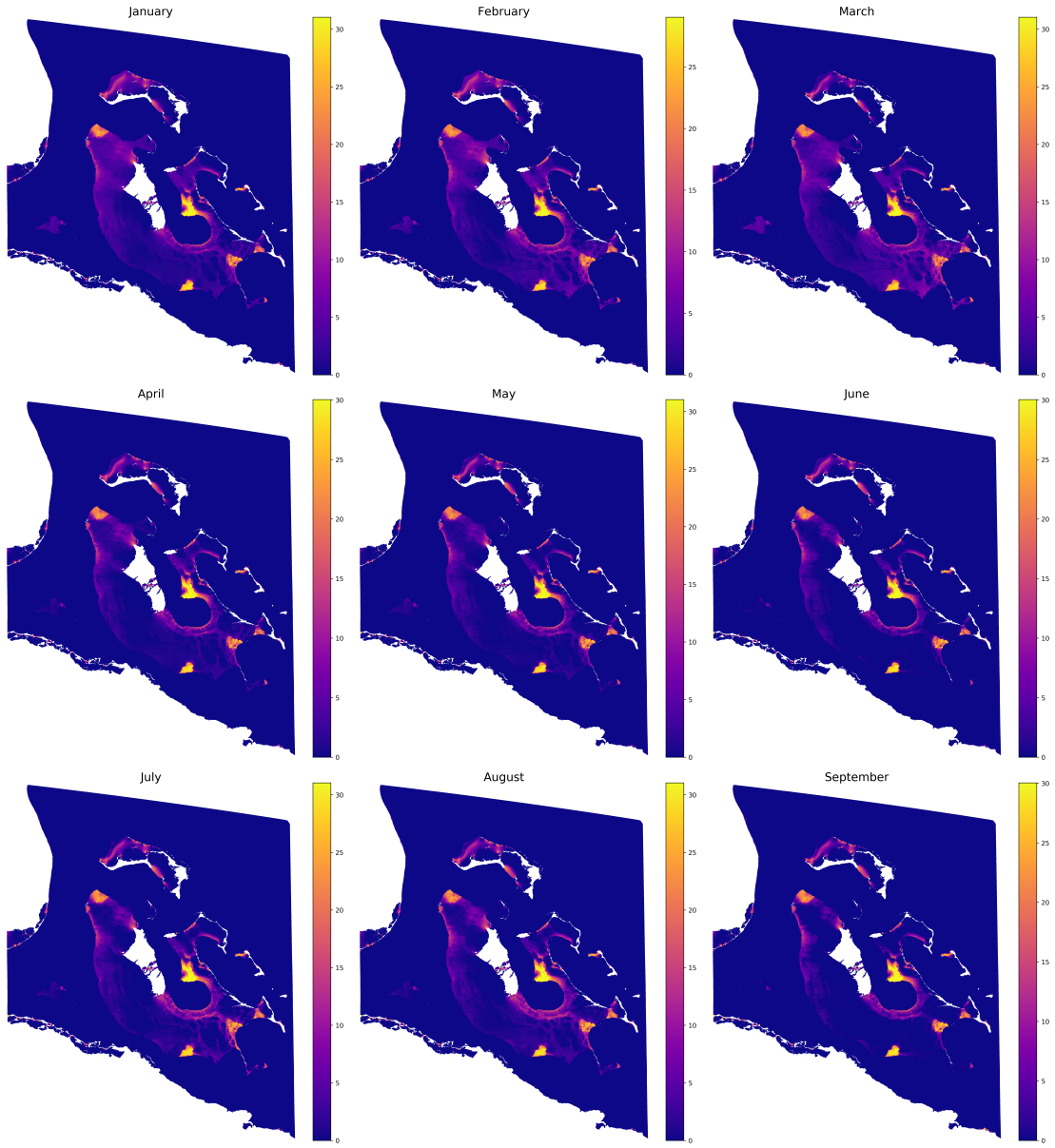

Fig. 4.1: Threshold velocity indicator for each month of simulation without wetting-drying (2016). Units of the color bar are days

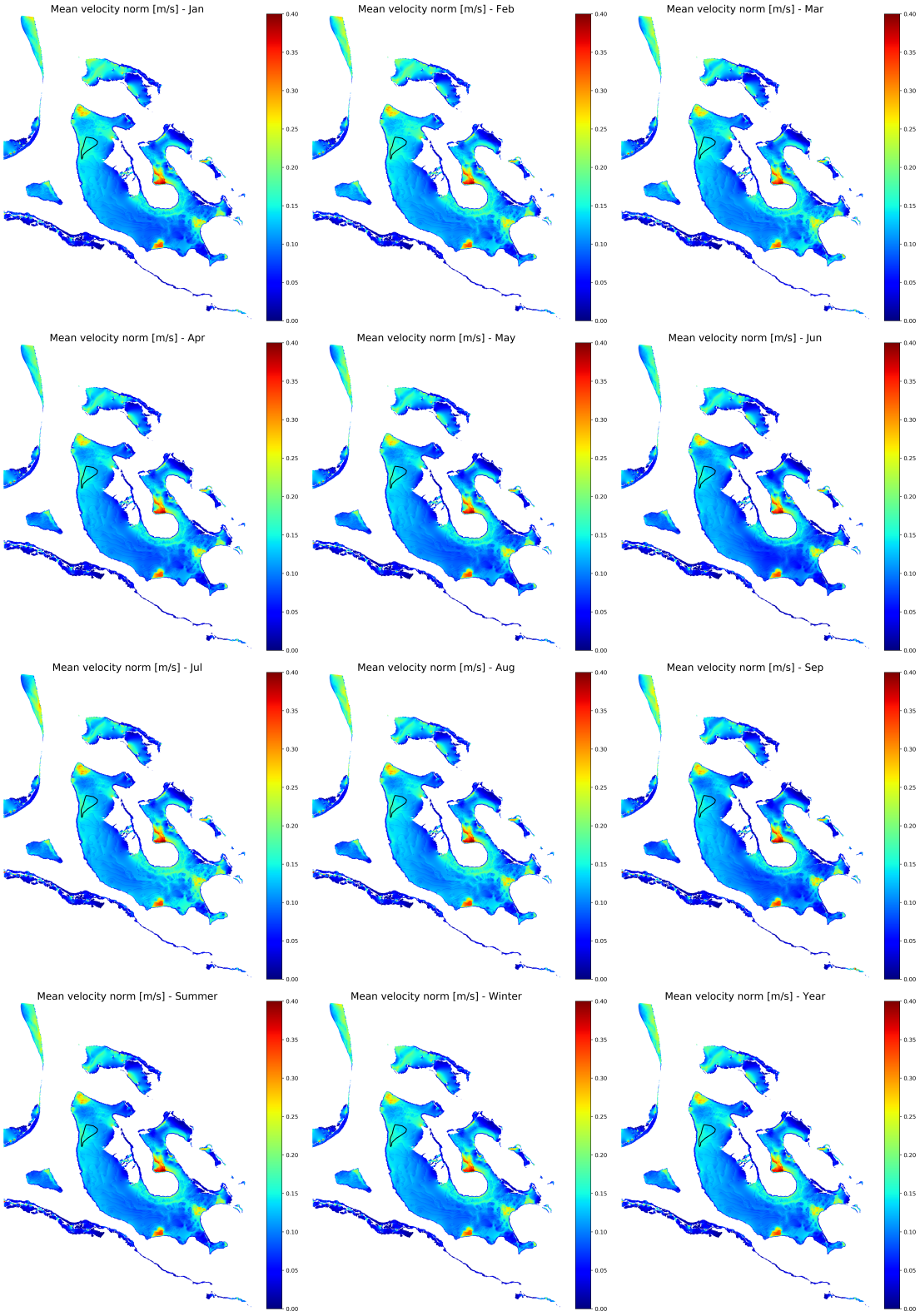

Fig. 4.2: Mean norm of the velocity for each month of simulation without wetting-drying (2016)

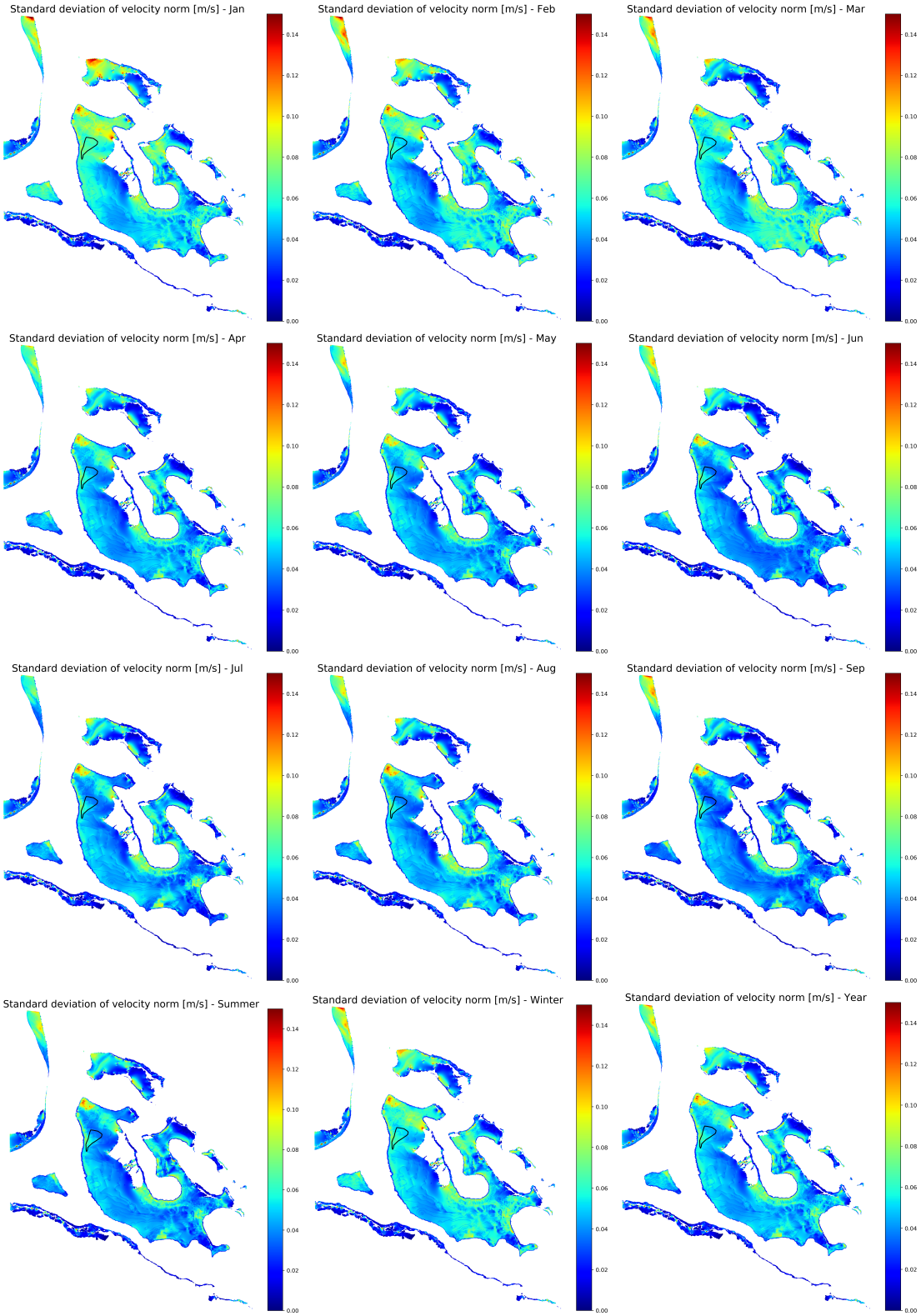

Fig. 4.3: Standard deviation of the norm of the velocity for each month of simulation without wetting-drying (2016)

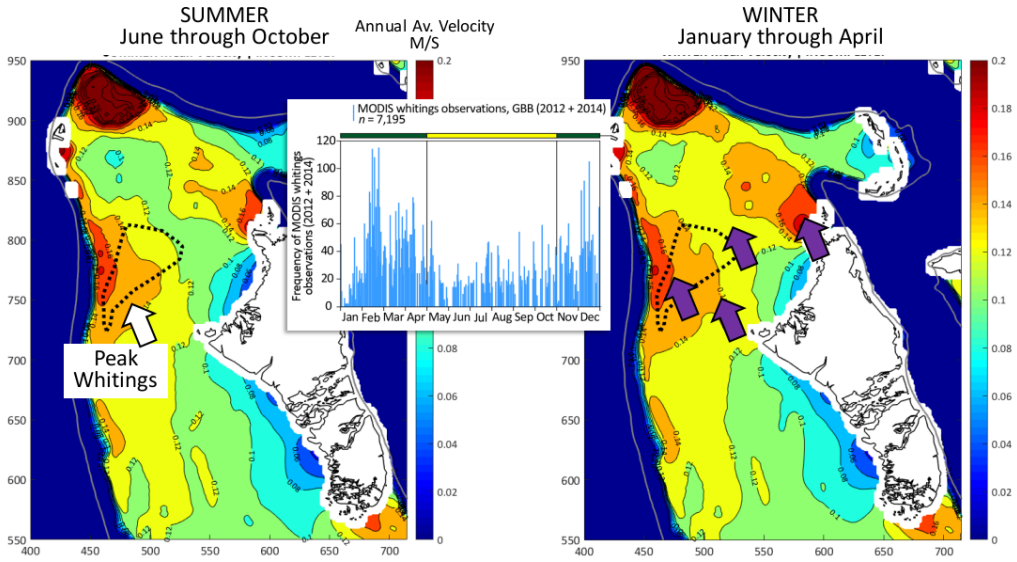

Fig. 4.4: Summer and winter contoured average annual flow velocities obtained after application of 9x9 pixel median filter on SLIM output without wetting-drying by Sam Purkis.

4.2 Water chemistry indicator

4.2.1 Lagrangian Particle Tracker

Concerning general motions of deep water particles, most of the particles of the Florida Straits are drifted up north due to the impact of the Florida Current and the Gulf Stream. However, a part of the particles seeded between Cay Salt Bank and Cuba are drifted to the southeast through Old Bahama Bank. This is illustrated by velocity field of figure 4.5. Particles seeded north to Little Bahama Bank and in Northwest Providence Channel are also transported to the northwest under the influence of the Gulf Stream.

Regarding shallow water particles dynamics, blue particles seeded at the southern margin of Cay Sal Bank are grabbed by the currents shown on figure 4.5 and are then brought up north along the western margin of the Great Bahama Bank. Shallow water particles on the northern margin of Little Bahamas Bank are also transported to the northwest under the impact of the water circulation north to Little Bahama Bank. On the other hand, waters from the Great Bahama Bank seem to flow a southwestward movement, drifting away from Tongue the Ocean and Berry Island to then agglomerate on the southwestern boundary of the bank However,the density of particles agglomerated on the western margin of the Bank is relatively lower at latitudes where whitings are observed, as shown in figure 4.6. Looking at the streamlines, one notices that at these latitudes, northward currents are performing an "about-turn", pointing toward the interior of the platform before pointing south. Moreover, lower particle density at these latitudes is consistent with the relatively higher velocity norms observed on figure 4.2. Finally, particles seeded on the northwestern tip of the bank are also transported northward by the Gulf Stream, while particles in vicinity of Old Bahama Channel are brought out of bank southeastward by currents shown in figure 4.5.

Few particle mixing is observable on the bank. On the western boundary of the GBB, this seems to be due to the fact that currents drain deep water particles either northward our southeastward tangentially to the platform margin, which only permits very limited particle exchanges. However, weaker blue particle density in the vicinity of Bimini Islands suggests that off-platform waters enter the bank in these regions. On the other hand, at the interface with Tongue of the Ocean, where particle dynamics shows that off-platform waters enter the shelf

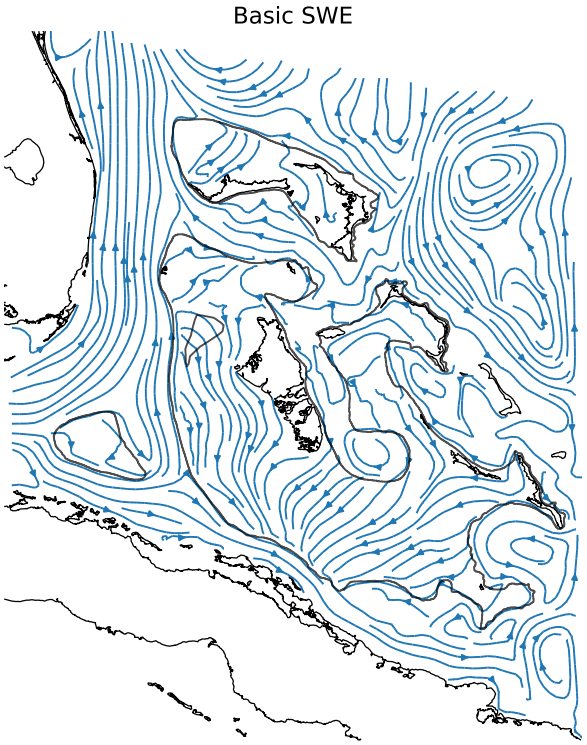

Fig. 4.5: Mean velocity field simulated for January 2016 without wetting-drying

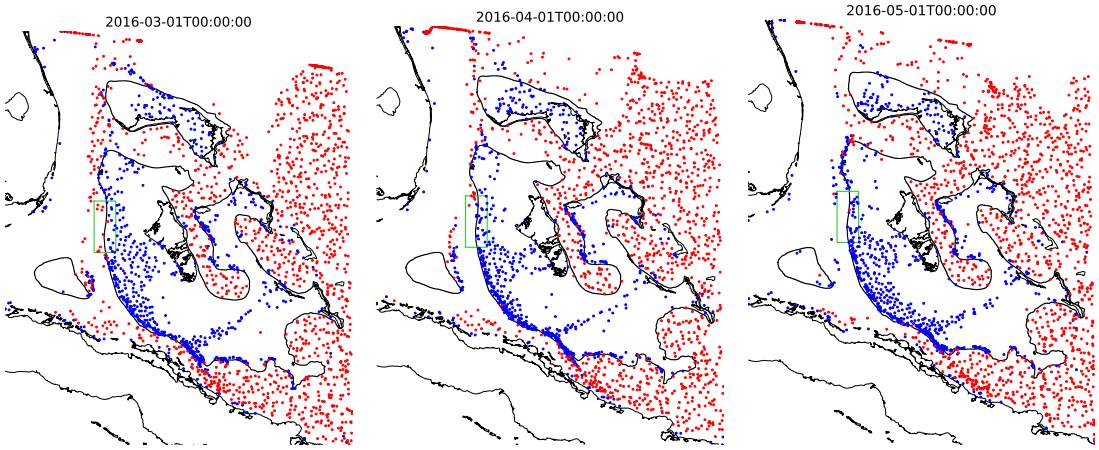

Fig. 4.6: Examples showing the lower shallow water particles density at the end of the month between 24.25 N and 25.2N on the western GBB margin

break, this absence of observable mixing is due to the water depth in TOTO. Only a relatively small fraction of the deep water column enters the shallow bank. This therefore explains why we see more shallow water particles leaving the bank than deep water particles entering the bank, even though shallow particle motions on the bank clearly indicate that off-platform waters enter the bank.

Nonetheless, it is punctually possible to observe some deep water particles entering the Great Bahama Bank in the region of Old Bahama Channel and Northwest providence Channel (see right subfigure of figure 4.6) and in the zone located at whitings latitudes (see left subfigure of figure 4.6). These last particles mostly enter the platform south to whitings area and are then brought up north by currents.

4.2.2 Mean volume flow rate through the 30m isobath

Information on the monthly mean flow rate is consistent with most of observed particle motions. For instance, the western margin of Tongue of the Ocean is dominated by platformward fluxes while most of seaward fluxes are observed on the western margin of the Great Bahama Bank (especially in the southwest). This implies that water enters the bank east, at Tongue of the Ocean and mostly leaves it through the southwestern and northwestern parts of the platform margin, flowing into the Florida Straits. This is consistent with the observed movement of the particles on the platform and the velocity field. Moreover, important seaward fluxes are observed in the vicinity of Old Bahama Channel and on the northwestern tip of the Great Bahama Bank, which are the two main locations where shallow water particles were leaving the Great Bahama Bank. Large platformward fluxes on the southern tip of Tongue of the Ocean is also consistent with the fact that this region is the largest high-energy sand deposit on Earth. On the other hand, seaward and platformward fluxes through the western margin of the bank are way smaller at the latitudes of Andros Island. Looking at figure 4.5, one notices that streamlines in these regions are tangent to the platform margin inside and outside the bank, while seaward and platformward streamlines are observed in the southwestern and northwestern parts of the platform margin respectively. Therefore, relatively few waters leave or enter the platform at these latitudes.

Coupling fluxes information with velocity field, we deduce that off-platworm waters mostly enter Great Bahama Bank:

- ◇ from Tongue of the Ocean and then flow southwestward and leaves the Bank into Old Bahama Channel
- ◇ in the vicinity of the Bimini Islands and then flow northeastward and leaves Great Bahama bank into Northwest Providence Channel
- ◇ through the western margin of Great Bahama Bank, south to Cay Sal Bank latitudes and are then brought by water circulation on the platform southward to Old Bahama Channel
- ◇ through the western margin of Great Bahama Bank, at the latitudes of Andros Islands. These waters are then brought northward by water circulation on the platform until they reach the latitudes of the whitings hot spot.

Finally, one may notice that platformward fluxes are stronger during summer months than winter months. Off-platform waters being more saturated with respect to aragonite than platform-top ones, whitings formation seems then to be favored during summer months. However, these means are to be taken with a pinch of salt as some months are missing. Moreover, platformward fluxes of January are significantly stronger than the ones observed

during the rest of the year. This is pretty doubtful, as no significant difference is observed in velocity norms in January with respect to the rest of the year.

4.2.3 Age of waters

Using the Eulerian tracer of section 3.2.3 with Okubo formula and $\alpha = 0.003m^{0.85}s^{-1}$ during a 100 days simulation starting on 2016/01/01, we obtained the ages given in figure 4.8. The observed age distribution on Great Bahama Bank is fairly consistent with other indicator values. Presence on "younger" waters on the east and "older" ones on the western margin of the Bank matches the observed particle displacements. Moreover, the fact that new waters entering the platform near Berry Islands head then southward is consistent with the velocity field of figure 4.5. Furthermore, one notices a zone of slightly older waters in the south of the whitings hot spot (black shape on figure 4.8) that matches the zone of relatively higher mean velocity norm of figure 4.2 as well as the area presenting eastward pointing streamlines in figure 4.5. Looking at the shape of whitings hot spot, one notices that most of whitings seem to take place in younger waters, which is consistent with the fact that off-platform waters are more saturated with aragonite.

On the other hand, age distribution shows us that quite a significant part of off-platform waters enter Great Bahama Bank north to Andros Island, which is consistent with velocity field in figure 4.5. However, no platformward flux was observed in this region on figure 4.7. This suggests that our flux indicator might be missing some information.

Results of figure 4.8 do not match the ones of figure 3.4. The ages we obtain in the vicinity of Bimini Islands are way higher than the ones of [Broecker and Takahashi, 1966] while the ages we obtains in the near Andros Island are smaller. Nonetheless, just as in figure 3.4, older ages are located in the vicinity of Andros Island while younger edges are located near the platform margin. Moreover, shape of contour lines on figure 3.4 suggests that new waters mostly enters the bank through its eastern margin, which is also what one observes on figure 4.8. Finally, our results suggest that water has a relatively young age on the vast majority of the platform, which is irreconcilable with ^{13}C enrichment.

4.2.4 Water chemistry indicators: summary

Volume flow rate through the 30m isobath as well as particle tracker show that pretty few off-platform waters enter the bank through its western margin at whitings latitude. However, under the action of the Gulf Stream, off-platform waters entering the bank south to whitings zone are driven north by water circulation. On the other hand, age of waters shows that most of whitings occur in a region of relatively young waters that entered the bank north to Andros Island, even though such platformward fluxes are not visible on our fluxes figures. Seasonal variation of the flux (although dubious as data are missing for thee months) shows that more off-platform waters enter Great Bahama Bank through its western margin during summer, which seems to favor whitings occurrence during summer months. However, considering age of waters and the shape of whitings occurrence area, off-platform waters entering Great Bahama Bank through its eastern margin seem to play a more significant role in whitings formation. Therefore, seasonal variation of this flux might be causing seasonal variation of whitings frequency. Unfortunately, as this flux was not taken into account by our fluxes indicator, we could not estimate its impact and seasonal variation.

Finally, age of waters shows that water has a relatively short residence time on most of the shelf break, which contradicts results of [Broecker and Takahashi, 1966] as well as the hypothesis of water productivity being the origine of ^{13}C enrichment.

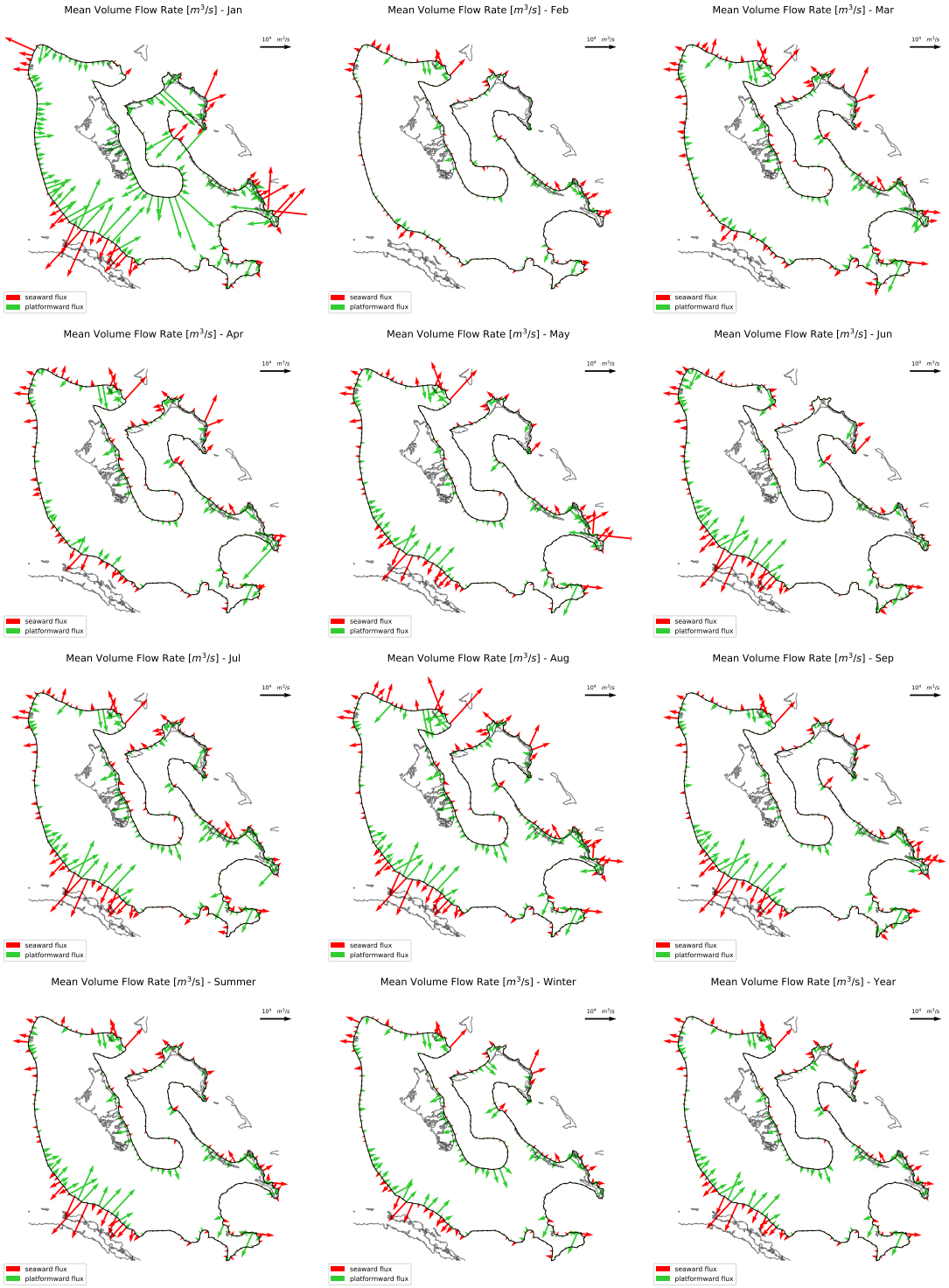

Fig. 4.7: Mean volume flow rate through the 30m isobath for each month of simulation (2016)

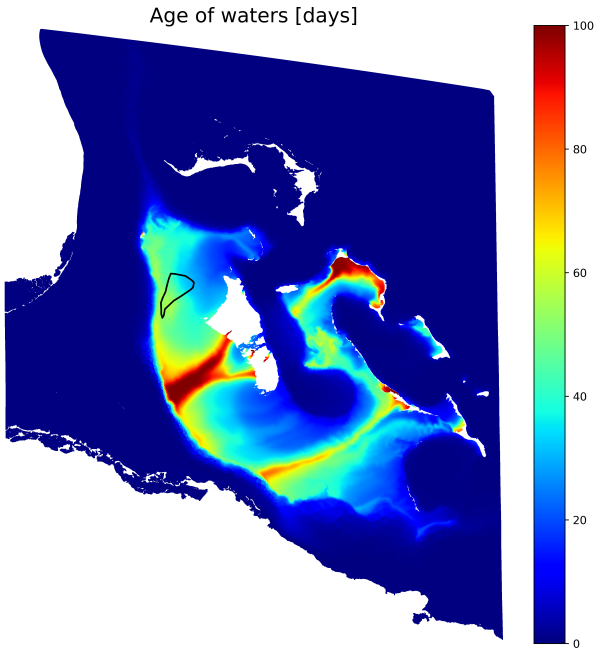

Fig. 4.8: Age of waters after 100 simulated days using basic shallow water equations

5 Wetting-drying: results

As 70% of whitings occur during winter, we were missing information of significant importance not being able to simulate the last three months of 2016. Therefore, we used wetting drying methods to perform a simulation of the full year. The obtained results differed from the ones obtained using classic shallow water equation in numerous ways. These new results are discussed in the following section

5.1 Resuspension indicators

First of all, one may observe on figure 5.1 that the mean norm distribution really differs with or without wetting-drying. Mean velocity on Great Bahama bank is way higher, especially on the western margin. Velocity seems to be less dissipated by friction on the declivities surrounding Great Bahama Bank. This result was fairly counterintuitive as the absence of strong platformward flux south to Tongue of the Ocean suggested that velocity field was more dissipated by slope-dependent frictions with wetting-drying methods. However, we emit the hypothesis that this reduced dissipative behavior obtained using wetting-drying could be due to Smagorinsky viscosity parametrization. IndeNorhed, modified shallow water equation are solved under conservative form in SLIM wetting-drying scheme [Kärnä et al., 2011], i.e. with H and $H\mathbf{u}$ as state variables. Therefore, Smagorinsky viscosity, expressed as function of $\nabla\mathbf{u}$ in the non conservative form of the shallow waters equations 2.4 is expressed as a function of $\nabla(H\mathbf{u})$ in the conservative form. Furthermore, large variations ΔH of the water column depth H have an important impact on the velocity field $\mathbf{u}$ while, on the other hand, the impact on $H\mathbf{u}$ is fairly negligible due to mass conservation. Consequently, Smagorinsky viscosity strongly increases in regions presenting a sharp bathymetry gradient in non conservative form while its value is weakly impacted in conservative form. This would suggest that wetting-drying scheme is more accurate in this regard.

On the other hand, some features remain unchanged. For instance, time variation of the mean velocity norm is once again fairly negligible while a zone of relatively higher velocity norm remains observable on whitings hot spot (in black in figure 5.1). However, no significant difference in mean velocity norm is observable between summer and winter months (see figure 5.2).
Standard deviation of the velocity norm is also higher (see figures A.2 and A.1) using wetting-drying methods. Highest values being, as for the mean norm, located on the western margin of Great Bahama Bank, with no strong variation through time. Threshold velocity indicator values for winter and summer month (figure 5.2) are consistent with mean velocity norms. High values of the indicator are observed in the region where whitings are observed (as well as all along the western margin of the bank) and no strong difference is noticeable between summer and winter, implying that sediment resuspension is evenly likely all year long.

Just as in our first approach, presence of zones of high velocity norm with relatively important standard deviation in the vicinity of regions where whitings are observed goes in the sense of bottom resuspension in these regions ([Boss and Neumann, 1993]). Nonetheless, seasonal variation of velocity is here smaller than in our previous simulation. Therefore, although wetting-drying results suggest that bottom sediment resuspension might actually be part of whitings formation mechanism, it is not its driving process. Once again, one must investigate water exchanges between top-platform and off-platform waters to determine whether water chemistry can explain seasonal pattern of whitings frequency.

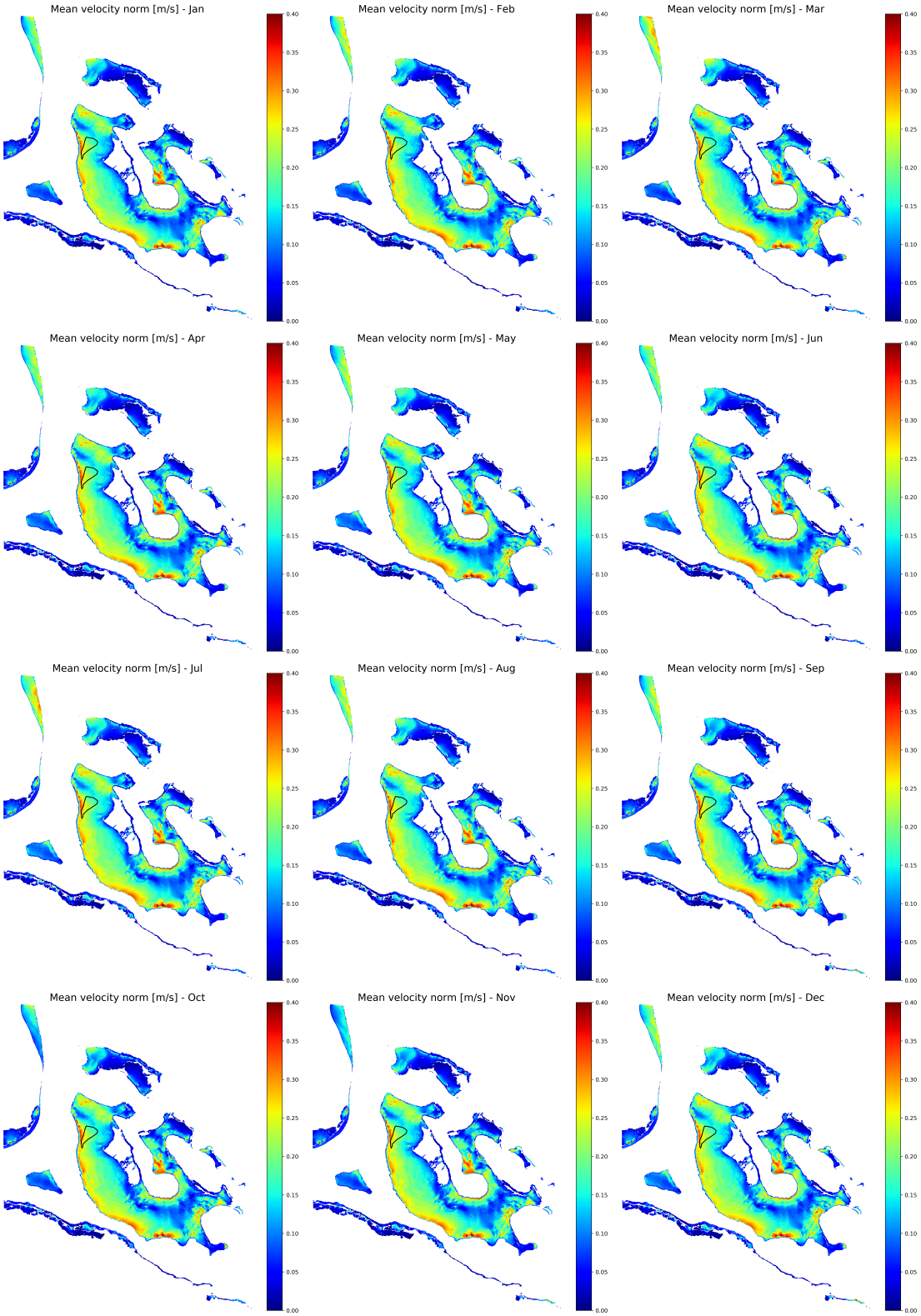

Fig. 5.1: Mean norm of the velocity for each month of simulation using wetting-drying with $C_S = 5$ (2016)

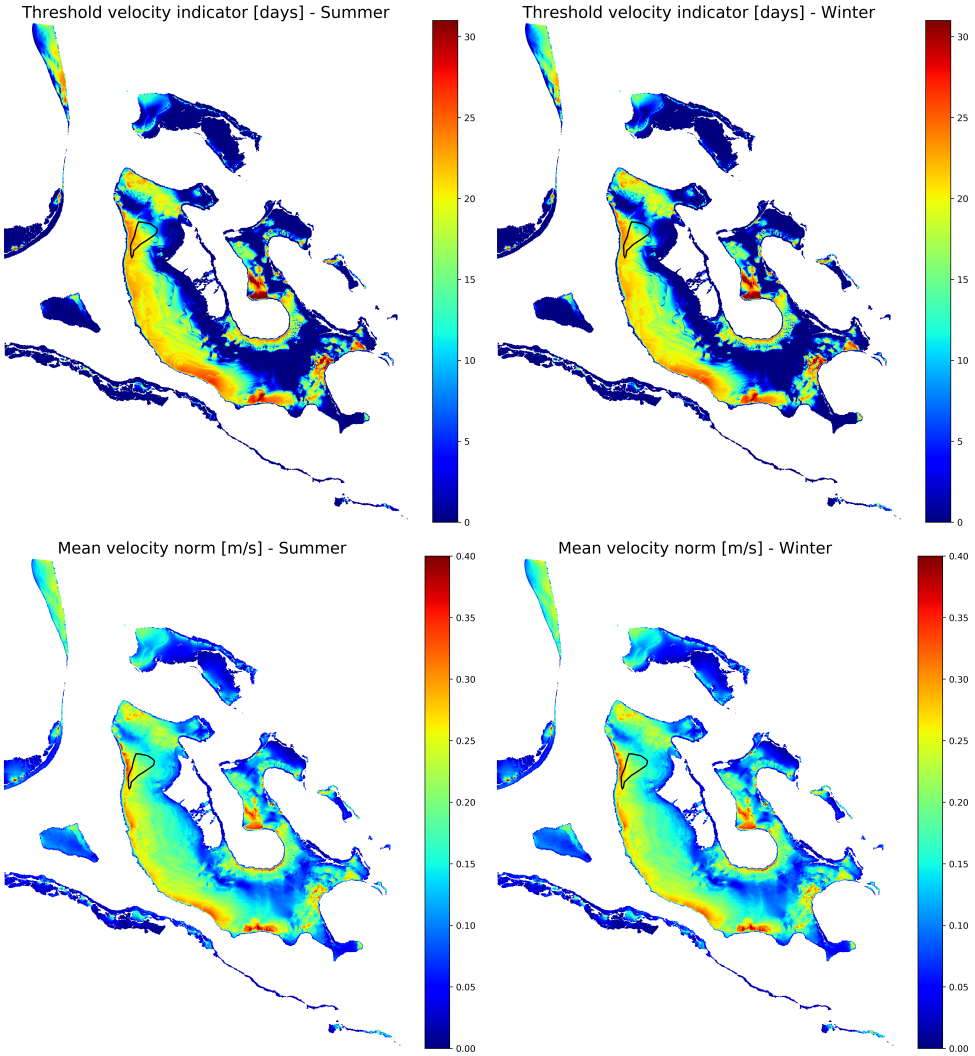

Fig. 5.2: Threshold velocity indicator and mean velocity norm for summer and winter months using wetting-drying methods with $C_S = 5$

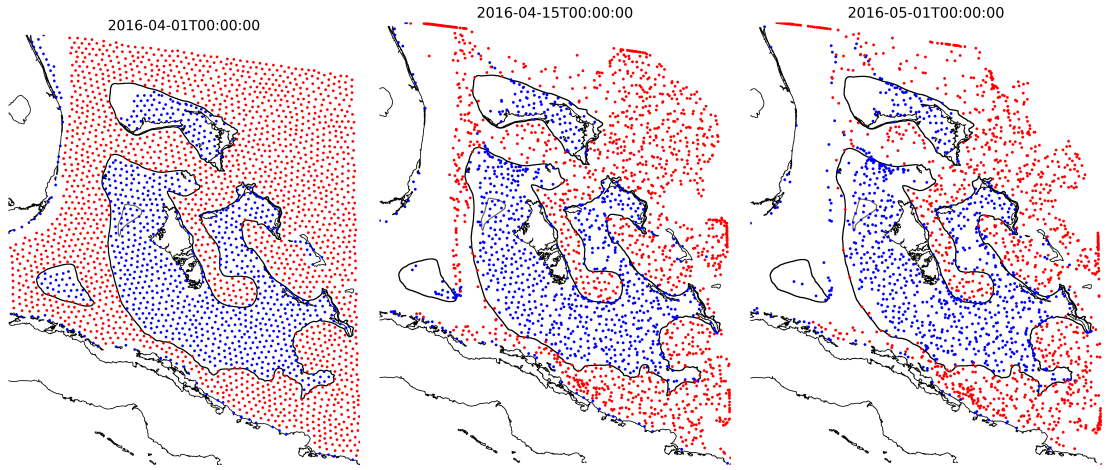

Fig. 5.3: Dispersal of deep water (red) and shallow water (blue) particles during April 2016 using wetting-drying with $C_S = 5$

5.2 Water chemistry indicators

5.2.1 Lagrangian Particle Tracker

Particle dynamics on Great Bahama Bank shown in figure 5.3 is here fairly differing from the one of figure 3.3. While particles previously had a general westward motion on the platform in the first simulation and then agglomerated on the western margin of the bank, they are now relatively static, going back and forth with tidal cycles with a slight eastward displacement south to Andros island, generating a small agglomeration of particles on the southern end of Tongue of the Ocean, and with a northward motion north to Andros Island, causing agglomeration at the interface with Northwest Providence Channel. This difference in particle displacements is captured in figure 5.4. While streamlines in the vicinity of Tongue of the Ocean were all pointing to Old Bahama Channel with basic SWE, they are now all pointing to TOTO with wetting-drying. This is not the only difference. With our first approach, streamlines on the platform at the latitudes of Andros Islands were mostly pointing southward to Old Bahama Channel. Using wetting-drying, these streamlines now originate from Andros Island and are either pointing northward to Northwest Providence Channel or southward to Old Bahama Channel. On the other hand, particles displacements and streamlines are similar outside of Great Bahama Bank in both simulations. This is due to boundary conditions and relaxation to HYCOM.

As in the first simulation, few particle mixing is observable on the Great Bahama Bank even though shallow particles motion strongly suggest that off-platform waters mainly enter the bank from the Florida Straits, through the western margin of the platform as well as through its eastern margin, north to Andros Island. As the motion of shallow water particles is now fairly uniformly eastward all along the western margin of the Great Bahama Bank, we no longer have occurrence of a special behavior at the latitudes were whitings take place as it was the case with previous results. Nonetheless, presence of higher mean velocity norms at the whitings hot spot shown in figure 5.1 suggests that there might have more off-platform waters entering the shelf break in this area. Finally, particles dynamics now advocates for all year long water mixing on the western part of the platform.

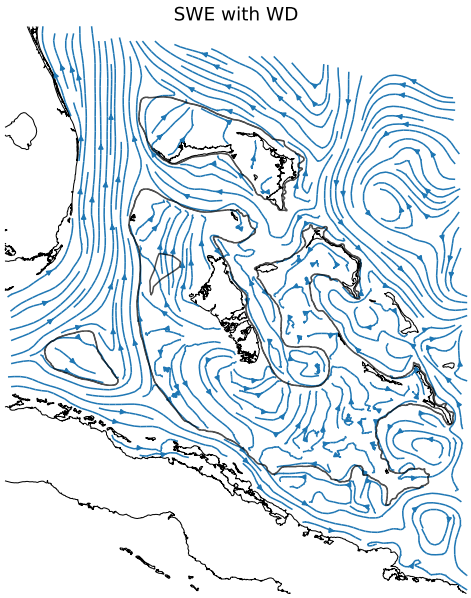

Fig. 5.4: Mean velocity field for the year 2016 obtained with wetting-drying and $C_S = 5$

5.2.2 Mean volume flow rate through the 30m isobath

The most obvious difference between the results of figure 5.5 and the previously obtained ones (figure 4.7) is the flux south to Tongue of the Ocean. While a relatively strong platformward flux was maintained all year long in figure 4.7, we now have a relatively weak seaward flux taking place all year long in figure 5.5. This matches particles agglomeration and seaward pointing streamlines previously observed at the southern tip of Tongue of the Ocean. This behavior is pretty dubious since the TOTO area is known to be the largest accumulation of ooid sand bodies on earth [Rankey and Reeder, 2011]. Such sands can only form in areas of sustained and strong flow as they must be frequently in motion to obtain their symmetric carbonate coatings. Hence, although relatively larger mean velocity norms south to TOTO are consistent with the presence of ooid sand bodies, the absence of any strong flux is on the other hand irreconcilable. Moreover, seaward and platformward fluxes through the western margin of the platform in the vicinity of Old Bahama Channel are weaker using wetting-drying. This is fairly surprising as larger mean velocity values on the western margin of the platform were expected to originate from larger fluxes. Moreover, as no more water from Tongue of the Ocean is brought to Old Bahama Channel, we do not have particle agglomeration on the southwestern shelf break margin anymore. On the contrary, particle motions in figure 5.3 suggest that platformward fluxes dominate in the area near Old Bahama Channel and that waters mostly enter the bank in this area.
Fluxes confirm what the particle tracker suggested in the last section: off-platform waters mainly enter Great Bahama Bank through its western margin. However, water circulation seems to show that these waters do not penetrate deep inside the platform as mean velocity field pushes them back to the Florida Straits. This balance between platformward fluxes and seaward velocity field on the western part of Great Bahama Bank might therefore explain the more "static" behavior of particles obtained with wetting-drying methods.

Furthermore, platformward fluxes are more important during summer months than during winter months (see figure 5.6). This once again suggests that whitings should be more likely to occur during summer. However, with wetting-drying, one no longer observes streamlines driving water flowing through the western margin of Great Bahama Bank northward to whitings latitudes. Therefore, one should mainly consider platformward fluxes at whitings

latitudes. These fluxes do not show any strong seasonal variation between winter and summer. However, seaward fluxes at whitings latitudes are slightly smaller during winter months, which could potentially enhance off-platform penetration on the Bank during winter.

5.2.3 Age of waters

Using the Eulerian tracer defined in section 3.2.3 is not straightforward as wetting-drying methods solve the conservative form of the modified shallow water equations. Implementing the tracer in a proper way being impossible due to lack of time, we tried an alternative approach, using the hourly η and $\mathbf{u}$ outputs of our wetting-drying methods as arguments of a non conservative Eulerian tracer. This implementation of the tracer presents several drawbacks. First of all, it sets the time integration time step to 1 hour, which is very large. Therefore, our integration quadrature may not converge. A solution to reduce the time step would then be to perform a (linear) interpolation of the velocity field between two outputs. This would then allow us to define n intermediary values of the velocity field between each hourly output and therefore reduce the integration time step to $3600/n$ seconds. However, even so, one has no guarantee of convergence of the time integration if n is not large enough. Moreover, this approach seem to be fairly numerically unstable as we obtained very dubious results, that did not match the values of any of he above cited indicators. This is why we have no result to show for water ages with wetting drying.

Still, based on particles motion and mean velocity fields, one could expect age of waters to follow a pattern similar the the one of figure 3.4, with young ages in the north of the shelf break and older ages at the latitides of Andros Island.

5.2.4 Wetting-drying without slope-dependent friction

Even though the results of the wetting-drying method presented high mean velocity norm in the area of the ooid sand bodies of Tongue of the Ocean, the absence of platformward flux in this region was irreconcilable with observations and literature. We therefore performed a new simulation with wetting-drying with slope-dependent friction parameter C_S set to 0. However, by lack of time, we only performed this simulation for January 2016. The obtained results for our different indicators is given in figure 5.7. One notices that we now have presence of a weak platformward flux in the area of Tongue of the ocean. Moreover, streamlines show that there is water circulation going from TOTO to Old Bahama Channel. Nonetheless, these fluxes are pretty weak compared to the ones observed without wetting-drying. This once again is pretty counterintuitive as there is no slope-dependent friction term to dissipate velocity flow coming from Tongue of the Ocean on the declivity boarding Great Bahama Bank. Moreover, as velocity norm on the ooid sand bodies is higher than the one observed without wetting-drying, one would expect stronger platformward fluxes. Taking a closer look at Tongue of the Ocean, we observe that mean velocity norm on the 30m isobath is relatively weak and then increases along the shelf break (see figure 5.8). Therefore, computing flux through the 30m isobath might be misleading and computing the flux through the 20m or 10m (or even shallower) isobath might give us a better picture of the currents.

Furthermore, one can observe that streamlines at latitudes where whitings are observed are roughly parallel to the east-west axis, which corresponds to the observed movements of whitings under the effect of wind driven currents. Therefore, the wetting-drying simulation with $C_S = 0$ seems to be the most physically accurate simulation we have made until now as, in addition to its east-west orientation, velocity field has an accurate dissipative behavior due to time integration of the conservative form of the SWE.

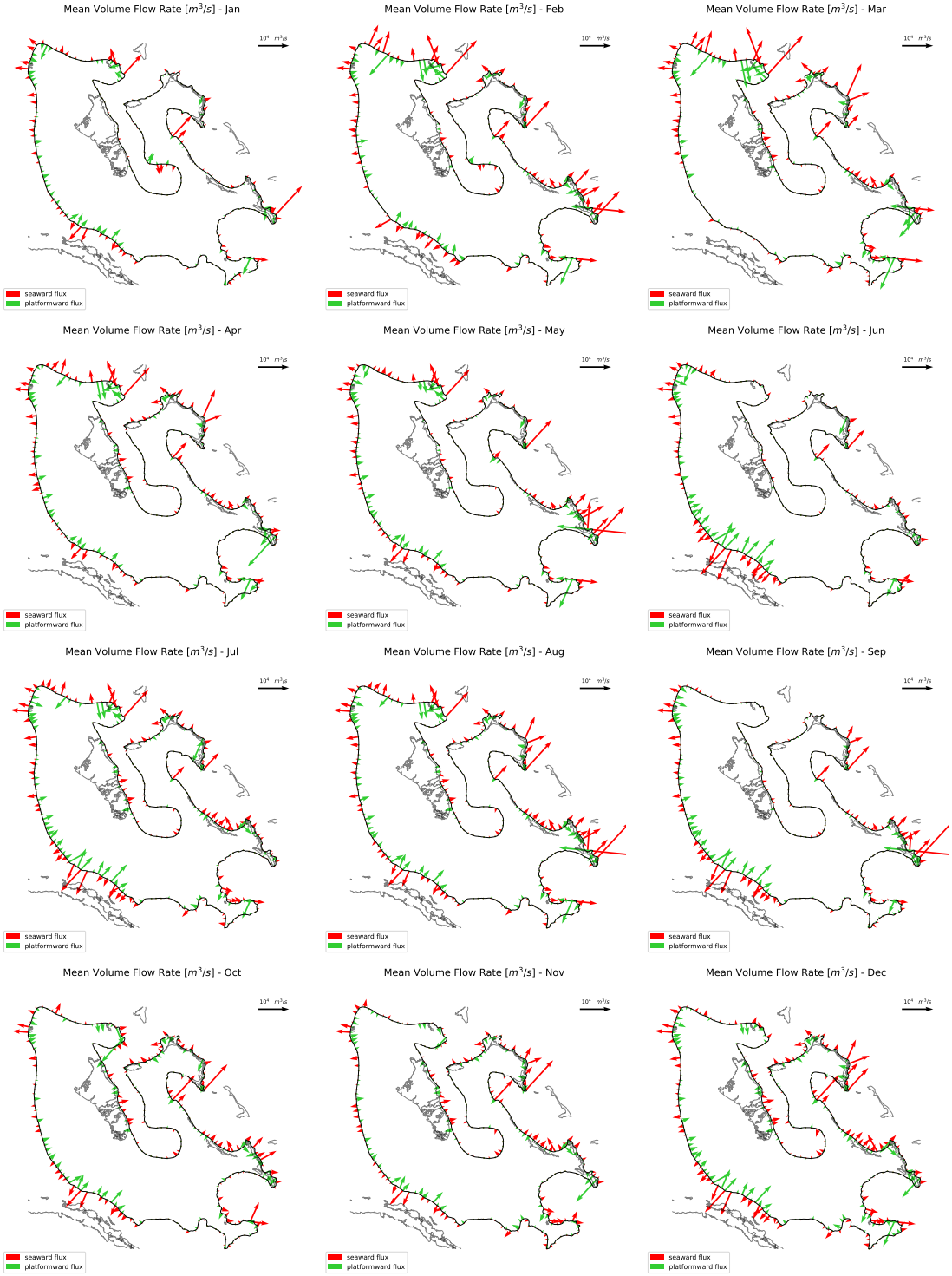

Fig. 5.5: Mean volume flow rate through the 30m isobath for each month of simulation using wetting-drying methods with $C_S = 5$ (2016)

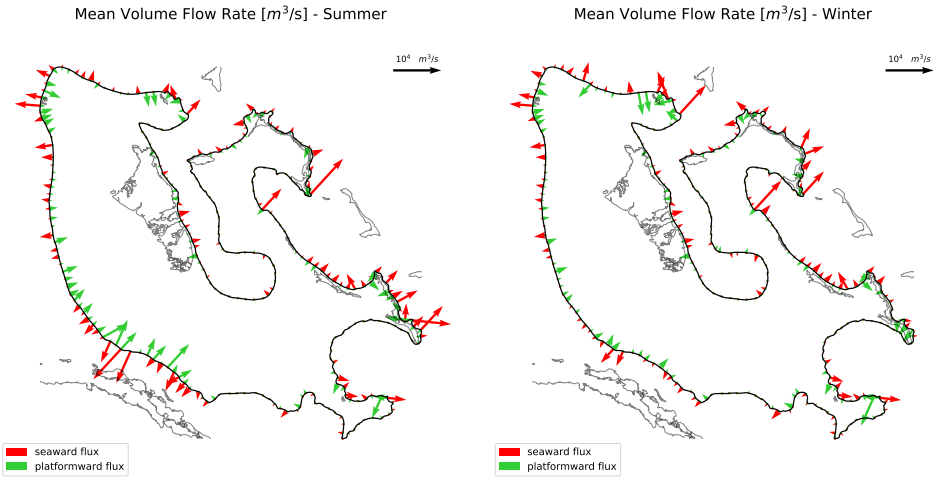

Fig. 5.6: Mean volume flow rate through the 30m isobath of summer and winter months using wetting-drying methods with $C_S = 5$

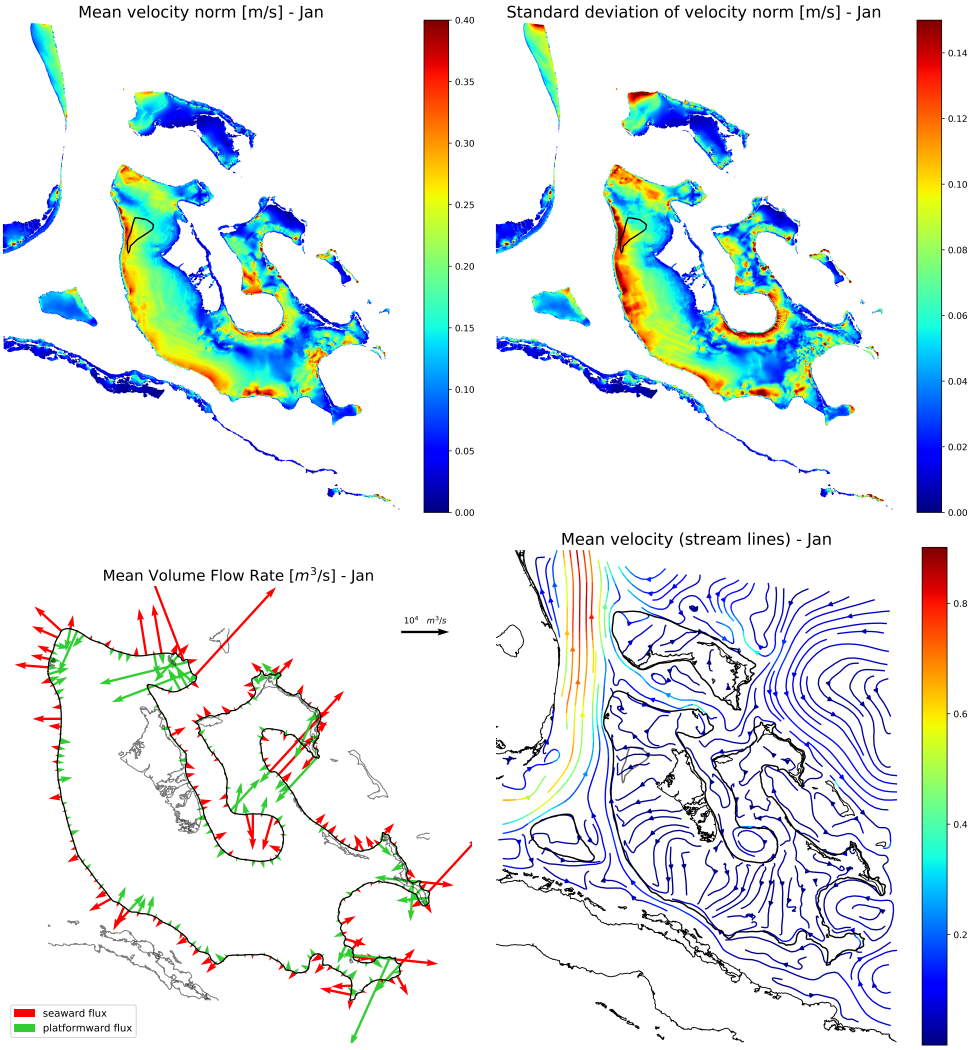

Fig. 5.7: Indicators computed from simulation using wetting-drying methods and $C_S = 0$. Units for streamlines are m/s.

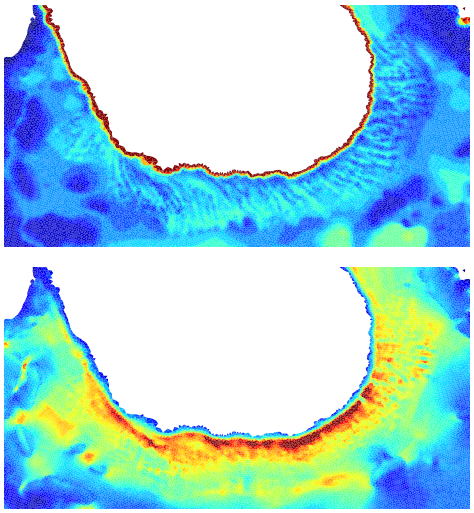

Fig. 5.8: Top: Zoom on bathymetry south to TOTO. One can distinguish ooid sand bodies. **Bottom**: Zoom on mean velocity norm south to TOTO. One notices weak norms on the 30m isobath and larger velocities on ooid sand bodies

5.2.5 Water chemistry indicators: summary

With wetting-drying methods and slope-dependent friction parameter $C_S = 5$, off-platform waters reaching whitings area are brought from the Florida Straits through the western margin of the bank. In opposition to what was observed in figure 4.8, no off-platform waters entering the shelf break north to Andros Island seem to attain whitings zone as mean velocity field drives them northward to Northwest Providence Channel. Moreover, off-platform waters coming from the Florida Straits do not seem the penetrate deep inside Great Bahama Bank as mean velocity field is pointing either northwestward or southwestward in figure 5.4. This is fairly inconsistent with the shape of whitings area (in black on figure 5.7), that is broader at its northeastern end. Furthermore, platformward fluxes are stronger during summer, which favors whitings occurrence during this period. Yet, based on mean velocity field in figure 5.4 , only off-platform waters entering the bank in the close neighborhood of whitings area should have an impact on whitings formation. As fluxes through the western margin of the bank at whitings latitude barely vary during the year, whitings formation does not seem to be enhanced by water exchanges during summer or winter. However, these results are pretty dubious as no platformward flux is observed south to Tongue of the Ocean and as fluxes are weaker than the ones of figure 4.7 despite the fact that mean velocity norms are larger in figure 5.1.

Finally, simulation with wetting-drying and $C_S = 0$ seemed to be more physically accurate as we now have presence of seaward fluxes south to Tongue of the Ocean as well as streamlines going from the area north to Andros Islands to whitings hot spot (figure 5.7). Moreover, figure 5.8 showed us that computing fluxes through the 30m isobath might be misleading as velocities increase along the shelf break.

6 Conclusion

Whitings, drifting patches of aragonite on the Great Bahama Bank, have been a sedimentological enigma for more than 80 years. Even though several models and mechanisms have been devised until now, no one has brought a satisfactory explanation of this phenomenon. However, it is assumed that the underlying mechanisms result from an in intricate bio-physico-chemical coupling between microbial communities, water circulation and chemistry. In this study, we used two different modeling approaches to perform a high-resolution simulation of hydrodynamics of the Great Bahama Bank. The obtained results were then used to investigate two main mechanisms. First, we tried to assess the presence of sufficiently high velocity norms to erode seabed and incur resuspension of bottom-sediments that could then be used as nucleation points for aragonite. Secondly, exchanges between off-platform and platform-top waters were investigated to study water saturation state with respect to aragonite on Great Bahama Bank as well as water residence time on the platform. As off-platform waters are more saturated with respect to aragonite, strong inflows of ocean waters on the shelf break favors whitings precipitation. On the other hand, the fact that whitings are mostly occurring during winter is fairly counterintuitive as thermodynamical laws state that most chemical and biological processes resulting in aragonite precipitation are enhanced by higher temperatures. Yet, interactions between warmer off-platform and colder platform-top waters might explain the increased whitings occurrence frequency during winter months. Finally, long residence time in Great Bahama Bank would explain ^{13}C enrichment of top-platform waters.

Regarding bottom-sediment resuspensions, both modeling approaches presented zones of larger mean velocity norm in the area where whitings are observed. According to [Neumann et al., 1970], these velocities were sufficient to erode seabed. Moreover, these high mean velocity norm areas were also presenting high standard deviation of currents velocity nom, which was also consistent with resuspension processes requiring significant current velocity variations [Boss and Neumann, 1993]. Furthermore, no strong seasonal variability of the mean and standard deviation of current velocity norm was observed during the year. This behavior, although quite dubious, implies that sediment resuspension is equally likely to happen all year long. Hence, although our results seem to show that bottom-sediment resuspension actually occur in whitings areas, it cannot explain difference of whitings occurrence frequency between seasons.

Concerning exchanges between off-platform and platform-top waters, the two modeling approaches were showing very different behaviors. Yet, both showed that off-platform waters from Florida Straits entering Great Bahama Bank through its western margin were not able to penetrate deep inside the shelf break. This fact, associated with the shape of the area where whitings are observed, seems to show that waters from the Straits have a fairly limited impact on whitings formation. This can then explain why whitings occur 70% more often during winter months despite the fact that platformward fluxes through the western margin of the bank are more important during summer. On the other hand, off-platform waters entering Great Bahama Bank north to Andros Island might play a more important role in water formation. However, these platformward fluxes were not studied as they were not properly handled by our model. Finally, regarding water age, this study brings pretty few information as age computed by our first model was quite irreconcilable with measurements of [Broecker and Takahashi, 1966] and as a proper conservative Eulerian tracer has to be implemented to accurately exploit results of wetting-drying simulation.

Although this study does not bring much new answers to the whitings enigma, it builds a basis and offers some tracks to pursue investigations. Indeed, despite the lack of measurement on Great Bahama Bank to accurately calibrate our model, the wetting drying approach with no slope-dependent friction term seems to be a fairly accurate setup as it combines a good

dissipative behavior with the presence of seaward fluxes south to Tongue of the Ocean, overcoming the weaknesses of the two modeling approaches detailed in this study. Moreover, it showed that by computing the fluxes through the 30m isobath, one might be missing some crucial information. Therefore, enhancing computation of platformward fluxes, we might be able to better understand the impact of off-platform waters entering the bank north to Andros Island, which would maybe give us a hint about the reason of higher whitings occurrence frequency during winter months.

References

[Aizinger and Dawson, 2002] Aizinger, V. and Dawson, C. (2002). A discontinuous galerkin method for two-dimensional flow and transport in shallow water. *Advances in Water Resources*, 25(1):67–84.

[Alonso et al., 2008] Alonso, R., Santillana, M., and Dawson, C. (2008). On the diffusive wave approximation of the shallow water equations. *European Journal of Applied Mathematics*, 19(5):575–606.

[Amante and Eakins, 2009] Amante, C. and Eakins, B. W. (2009). Etopo1 1 arc-minute global relief model: Procedures, data sources and analysis. *NOAA Technical Memorandum NESDIS NGDC-24. National Geophysical Data Center, NOAA*.

[Andutta et al., 2011] Andutta, F. P., Ridd, P. V., and Wolanski, E. (2011). Dynamics of hypersaline coastal waters in the great barrier reef. *Estuarine, Coastal and Shelf Science*, 94(4):299–305.

[Bates and Hervouet, 1999] Bates, P. D. and Hervouet, J.-M. (1999). A new method for moving–boundary hydrodynamic problems in shallow water. In *Proceedings of the Royal Society of London A: Mathematical, Physical and Engineering Sciences*, volume 455, pages 3107–3128. The Royal Society.

[Bathurst, 1972] Bathurst, R. G. (1972). *Carbonate sediments and their diagenesis*, volume 12. Elsevier.

[Bernard et al., 2007] Bernard, P.-E., Chevaugeon, N., Legat, V., Deleersnijder, E., and Remacle, J.-F. (2007). High-order h-adaptive discontinuous galerkin methods for ocean modelling. *Ocean Dynamics*, 57(2):109–121.

[Boss and Neumann, 1993] Boss, S. K. and Neumann, A. C. (1993). Physical versus chemical processes of "whiting" formation in the bahamas. *Carbonates and Evaporites*, 8(2):135.

[Broecker et al., 2000] Broecker, W., Sanyal, A., and Takahashi, T. (2000). The origin of bahamian whitings revisited. *Geophysical Research Letters*, 27(22):3759–3760.

[Broecker et al., 2001] Broecker, W. S., Langdon, C., Takahashi, T., and Peng, T.-H. (2001). Factors controlling the rate of caco3 precipitation on great bahama bank. *Global Biogeochemical Cycles*, 15(3):589–596.

[Broecker and Takahashi, 1966] Broecker, W. S. and Takahashi, T. (1966). Calcium carbonate precipitation on the bahama banks. *Journal of Geophysical Research*, 71(6):1575–1602.

[Bunya et al., 2009] Bunya, S., Kubatko, E. J., Westerink, J. J., and Dawson, C. (2009). A wetting and drying treatment for the runge–kutta discontinuous galerkin solution to the shallow water equations. *Computer Methods in Applied Mechanics and Engineering*, 198(17-20):1548–1562.

[Burchard et al., 2004] Burchard, H., Bolding, K., and Villarreal, M. R. (2004). Three-dimensional modelling of estuarine turbidity maxima in a tidal estuary. *Ocean Dynamics*, 54(2):250–265.

[Bustos-Serrano et al., 2009] Bustos-Serrano, H., Morse, J. W., and Millero, F. J. (2009). The formation of whitings on the little bahama bank. *Marine Chemistry*, 113(1):1–8.

[Carew and Mylroie, 1995] Carew, J. L. and Mylroie, J. E. (1995). Geology of the bahamas. *Bahamas Journal of Science*, 2(3):2–16.

[Castro et al., 2005] Castro, M. J., Ferreiro, A. F., García-Rodríguez, J. A., González-Vida, J. M., Macías, J., Parés, C., and Vázquez-Cendón, M. E. (2005). The numerical treatment of wet/dry fronts in shallow flows: application to one-layer and two-layer systems. *Mathematical and Computer Modelling*, 42(3-4):419–439.

[Casulli, 2009] Casulli, V. (2009). A high-resolution wetting and drying algorithm for free-surface hydrodynamics. *International Journal for Numerical Methods in Fluids*, 60(4):391–408.

[Cockburn and Shu, 2001] Cockburn, B. and Shu, C.-W. (2001). Runge–kutta discontinuous galerkin methods for convection-dominated problems. *Journal of scientific computing*, 16(3):173–261.

[Cushman-Roisin and Beckers, 2011] Cushman-Roisin, B. and Beckers, J.-M. (2011). *Introduction to geophysical fluid dynamics: physical and numerical aspects*, volume 101. Academic Press.

[de Brauwere et al., 2011] de Brauwere, A., De Brye, B., Blaise, S., and Deleersnijder, E. (2011). Residence time, exposure time and connectivity in the scheldt estuary. *Journal of Marine Systems*, 84(3-4):85–95.

[de Brye et al., 2013] de Brye, B., de Brauwere, A., Gourgue, O., Delhez, E. J., and Deleersnijder, E. (2013). Reprint of water renewal timescales in the scheldt estuary. *Journal of Marine Systems*, 128:3–16.

[De Brye et al., 2010] De Brye, B., de Brauwere, A., Gourgue, O., Kärnä, T., Lambrechts, J., Comblen, R., and Deleersnijder, E. (2010). A finite-element, multi-scale model of the Scheldt tributaries, river, estuary and ROFI. *Coastal Engineering*, 57(9):850–863.

[de Brye et al., 2011] de Brye, B., Schellen, S., Sassi, M., Vermeulen, B., Kärnä, T., Deleersnijder, E., and Hoitink, T. (2011). Preliminary results of a finite-element, multi-scale model of the mahakam delta (indonesia). *Ocean Dynamics*, 61(8):1107–1120.

[Defina, 2000] Defina, A. (2000). Two-dimensional shallow flow equations for partially dry areas. *Water resources research*, 36(11):3251–3264.

[Delhez et al., 2011] Delhez, E. J., Debrauwere, A., and Deleersnijder, E. (2011). Cart: the constituent-oriented age and residence time theory. In *International workshop/school on Tracer and Timescale Methods for Understanding Complex Geophysical and Environmental Processes*.

[Dimou and Adams, 1993] Dimou, K. N. and Adams, E. E. (1993). A random-walk, particle tracking model for well-mixed estuaries and coastal waters. *Estuarine, Coastal and Shelf Science*, 37(1):99–110.

[Döös et al., 2004] Döös, K., Nycander, J., and Sigray, P. (2004). Slope-dependent friction in a barotropic model. *Journal of Geophysical Research: Oceans*, 109(C1).

[Egbert and Erofeeva, 2002] Egbert, G. D. and Erofeeva, S. Y. (2002). Efficient inverse modeling of barotropic ocean tides. *Journal of Atmospheric and Oceanic Technology*, 19(2):183–204.

[Frys, 2017] Frys, C. (2017). Modeling marine connectivity in the Florida Coral Reef Tract. Master's thesis, Université Catholique de Louvain, Belgium.

[Geernaert, 1987] Geernaert, G. (1987). On the importance of the drag coefficient in air-sea interactions. *Dynamics of atmospheres and oceans*, 11(1):19–38.

[Gourgue et al., 2009] Gourgue, O., Comblen, R., Lambrechts, J., Kärnä, T., Legat, V., and Deleersnijder, E. (2009). A flux-limiting wetting–drying method for finite-element shallow-water models, with application to the scheldt estuary. *Advances in Water Resources*, 32(12):1726–1739.

[Harris et al., 2015] Harris, P. M. M., Purkis, S. J., Ellis, J., Swart, P. K., and Reijmer, J. J. (2015). Mapping bathymetry and depositional facies on great bahama bank. *Sedimentology*, 62(2):566–589.

[Heniche et al., 2000] Heniche, M., Secretan, Y., Boudreau, P., and Leclerc, M. (2000). A two-dimensional finite element drying-wetting shallow water model for rivers and estuaries. *Advances in Water Resources*, 23(4):359–372.

[Ip et al., 1998] Ip, J., Lynch, D., and Friedrichs, C. (1998). Simulation of estuarine flooding and dewatering with application to great bay, new hampshire. *Estuarine, Coastal and Shelf Science*, 47(2):119–141.

[Jiang et al., 2015] Jiang, L.-Q., Feely, R. A., Carter, B. R., Greeley, D. J., Gledhill, D. K., and Arzayus, K. M. (2015). Climatological distribution of aragonite saturation state in the global oceans. *Global Biogeochemical Cycles*, 29(10):1656–1673.

[Kärnä et al., 2011] Kärnä, T., De Brye, B., Gourgue, O., Lambrechts, J., Comblen, R., Legat, V., and Deleersnijder, E. (2011). A fully implicit wetting–drying method for dg-fem shallow water models, with an application to the scheldt estuary. *Computer Methods in Applied Mechanics and Engineering*, 200(5-8):509–524.

[Kuchinke et al., 2014] Kuchinke, M., Tilbrook, B., and Lenton, A. (2014). Seasonal variability of aragonite saturation state in the western pacific. *Marine Chemistry*, 161:1–13.

[Lambrechts et al., 2008] Lambrechts, J., Hanert, E., Deleersnijder, E., Bernard, P.-E., Legat, V., Remacle, J.-F., and Wolanski, E. (2008). A multi-scale model of the hydrodynamics of the whole great barrier reef. *Estuarine, Coastal and Shelf Science*, 79(1):143–151.

[Larson and Mylroie, 2012] Larson, E. B. and Mylroie, J. (2012). Infilled blue holes on the bahama banks as point sources for whiting origin. In *Geol Soc Am Abstracts with Programs*, volume 44, page 25.

[Larson and Mylroie, 2014] Larson, E. B. and Mylroie, J. E. (2014). A review of whiting formation in the bahamas and new models. *Carbonates and Evaporites*, 29(4):337–347.

[Le Bars et al., 2016] Le Bars, Y., Vallaeys, V., Deleersnijder, É., Hanert, E., Carrere, L., and Channelière, C. (2016). Unstructured-mesh modeling of the congo river-to-sea continuum. *Ocean Dynamics*, 66(4):589–603.

[Le Roux et al., 2005] Le Roux, D., Sene, A., Rostand, V., and Hanert, E. (2005). On some spurious mode issues in shallow-water models using a linear algebra approach. *Ocean Modelling*, 10(1):83–94.

[Marchandise and Remacle, 2006] Marchandise, E. and Remacle, J.-F. (2006). A stabilized finite element method using a discontinuous level set approach for solving two phase incompressible flows. *Journal of computational physics*, 219(2):780–800.

[Meyerhoff and Hatten, 1974] Meyerhoff, A. and Hatten, C. (1974). Bahamas salient of north america. In *The geology of continental margins*, pages 429–446. Springer.

[Milliman and Droxler, 1995] Milliman, J. D. and Droxler, A. W. (1995). Calcium carbonate sedimentation in the global ocean: linkages between the neritic and pelagic environments. *Oceanography*, 8(3):92–94.

[Milliman et al., 1993] Milliman, J. D., Freile, D., Steinen, R. P., and Wilber, R. J. (1993). Great bahama bank aragonitic muds: mostly inorganically precipitated, mostly exported. *Journal of Sedimentary Research*, 63(4).

[Morse et al., 2003] Morse, J. W., Gledhill, D. K., and Millero, F. J. (2003). Caco 3 precipitation kinetics in waters from the great bahama bank:: Implications for the relationship between bank hydrochemistry and whitings. *Geochimica et Cosmochimica Acta*, 67(15):2819–2826.

[Mucci and Morse, 1983] Mucci, A. and Morse, J. W. (1983). The incorporation of mg2+ and sr2+ into calcite overgrowths: influences of growth rate and solution composition. *Geochimica et Cosmochimica Acta*, 47(2):217–233.

[Neumann et al., 1970] Neumann, A. C., Gebelein, C. D., and Scoffin, T. P. (1970). The composition, structure and erodability of subtidal mats, abaco, bahamas. *Journal of Sedimentary Research*, 40(1).

[Nielsen and Apelt, 2003] Nielsen, C. and Apelt, C. (2003). Parameters affecting the performance of wetting and drying in a two-dimensional finite element long wave hydrodynamic model. *Journal of Hydraulic Engineering*, 129(8):628–636.

[Nikolos and Delis, 2009] Nikolos, I. and Delis, A. (2009). An unstructured node-centered finite volume scheme for shallow water flows with wet/dry fronts over complex topography. *Computer Methods in Applied Mechanics and Engineering*, 198(47-48):3723–3750.

[Okubo, 1971] Okubo, A. (1971). Oceanic diffusion diagrams. In *Deep sea research and oceanographic abstracts*, volume 18, pages 789–802. Elsevier.

[Rankey and Reeder, 2011] Rankey, E. C. and Reeder, S. L. (2011). Holocene oolitic marine sand complexes of the bahamas. *Journal of Sedimentary Research*, 81(2):97–117.

[Remacle et al., 2006] Remacle, J.-F., Frazao, S. S., Li, X., and Shephard, M. S. (2006). An adaptive discretization of shallow-water equations based on discontinuous galerkin methods. *International journal for numerical methods in fluids*, 52(8):903–923.

[Riviere, 2008] Riviere, B. (2008). *Discontinuous Galerkin methods for solving elliptic and parabolic equations: theory and implementation*. SIAM.

[Robbins and Blackwelder, 1992] Robbins, L. and Blackwelder, P. (1992). Biochemical and ultrastructural evidence for the origin of whitings: a biologically induced calcium carbonate precipitation mechanism. *Geology*, 20(5):464–468.

[Robbins et al., 1997] Robbins, L., Tao, Y., and Evans, C. (1997). Temporal and spatial distribution of whitings on great bahama bank and a new lime mud budget. *Geology*, 25(10):947–950.

[Robbins et al., 1996] Robbins, L., Yates, K., Shinn, G., and Blackwelder, P. (1996). Whitings on the great bahama bank: a microscopic solution to a macroscopic mystery. *Bahamas Journal of Science*, 4(1):2–7.

[Saha et al., 2010] Saha, S., Moorthi, S., Pan, H.-L., Wu, X., Wang, J., Nadiga, S., Tripp, P., Kistler, R., Woollen, J., Behringer, D., et al. (2010). The ncep climate forecast system reanalysis. *Bulletin of the American Meteorological Society*, 91(8):1015–1057.

[Saha et al., 2014] Saha, S., Moorthi, S., Wu, X., Wang, J., Nadiga, S., Tripp, P., Behringer, D., Hou, Y.-T., Chuang, H.-y., Iredell, M., et al. (2014). The ncep climate forecast system version 2. *Journal of Climate*, 27(6):2185–2208.

[Santillana and Dawson, 2010] Santillana, M. and Dawson, C. (2010). A local discontinuous galerkin method for a doubly nonlinear diffusion equation arising in shallow water modeling. *Computer Methods in Applied Mechanics and Engineering*, 199(23-24):1424–1436.

[Schwanenberg and Harms, 2004] Schwanenberg, D. and Harms, M. (2004). Discontinuous galerkin finite-element method for transcritical two-dimensional shallow water flows. *Journal of Hydraulic Engineering*, 130(5):412–421.

[Shinn et al., 1989] Shinn, E. A., Steinen, R. P., Lidz, B. H., and Swart, P. K. (1989). Whitings, a sedimentologic dilemma: Perspectives. *Journal of Sedimentary Research*, 59(1).

[Smagorinsky, 1963] Smagorinsky, J. (1963). General circulation experiments with the primitive equations: I. the basic experiment. *Monthly weather review*, 91(3):99–164.

[Smith and Banke, 1975] Smith, S. and Banke, E. (1975). Variation of the sea surface drag coefficient with wind speed. *Quarterly Journal of the Royal Meteorological Society*, 101(429):665–673.

[Sobey, 2009] Sobey, R. J. (2009). Wetting and drying in coastal flows. *Coastal Engineering*, 56(5-6):565–576.

[Spagnol et al., 2002] Spagnol, S., Wolanski, E., Deleersnijder, E., Brinkman, R., McAllister, F., Cushman-Roisin, B., and Hanert, E. (2002). An error frequently made in the evaluation of advective transport in two-dimensional lagrangian models of advection-diffusion in coral reef waters. *Marine Ecology Progress Series*, 235:299–302.

[Stelling and Duinmeijer, 2003] Stelling, G. S. and Duinmeijer, S. A. (2003). A staggered conservative scheme for every froude number in rapidly varied shallow water flows. *International journal for numerical methods in fluids*, 43(12):1329–1354.

[Thomas, 2015] Thomas, C. (2015). *Modelling marine connectivity in the Great Barrier Reef and exploring its ecological implications*. PhD thesis, Université Catholique de Louvain, Belgium.

[Thompson, 2000] Thompson, J. B. (2000). Microbial whitings. In *Microbial sediments*, pages 250–260. Springer.

[Van et al., 2016] Van, C. P., Gourgue, O., Sassi, M., Hoitink, A., Deleersnijder, E., and Soares-Frazão, S. (2016). Modelling fine-grained sediment transport in the mahakam land–sea continuum, indonesia. *Journal of hydro-environment research*, 13:103–120.

[Van't Hof and Vollebregt, 2005] Van't Hof, B. and Vollebregt, E. (2005). Modelling of wetting and drying of shallow water using artificial porosity. *International Journal for Numerical Methods in Fluids*, 48(11):1199–1217.

[Vincent et al., 2016] Vincent, D., Karatekin, Ö., Vallaeys, V., Hayes, A. G., Mastrogiuseppe, M., Notarnicola, C., Dehant, V., and Deleersnijder, E. (2016). Numerical study of tides in ontario lacus, a hydrocarbon lake on the surface of the saturnian moon titan. *Ocean Dynamics*, 66(4):461–482.

[Wells and Illing, 1964] Wells, A. and Illing, L. (1964). Present-day precipitation of calcium carbonate in the persian gulf. In *Developments in sedimentology*, volume 1, pages 429–435. Elsevier.

[Yates and Robbins, 1998] Yates, K. K. and Robbins, L. L. (1998). Production of carbonate sediments by a unicellular green alga. *American Mineralogist*, 83(11):1503–1509.

[Yuan et al., 2008] Yuan, D., Lin, B., and Falconer, R. (2008). Simulating moving boundary using a linked groundwater and surface water flow model. *Journal of hydrology*, 349(3-4):524–535.

[Zheng et al., 2003] Zheng, L., Chen, C., and Liu, H. (2003). A modeling study of the satilla river estuary, georgia. i: Flooding-drying process and water exchange over the salt marsh-estuary-shelf complex. *Estuaries*, 26(3):651–669.

[Zijlema and Stelling, 2008] Zijlema, M. and Stelling, G. (2008). Efficient computation of surf zone waves using the nonlinear shallow water equations with non-hydrostatic pressure. *Coastal Engineering*, 55(10):780–790.

[Zimmerman et al., 2009] Zimmerman, R. C., Burdige, D. J., et al. (2009). Optics and remote sensing of bahamian carbonate sediment whitings and potential relationship to wind-driven langmuir circulation. *Biogeosciences*, 6(3).

A Appendices

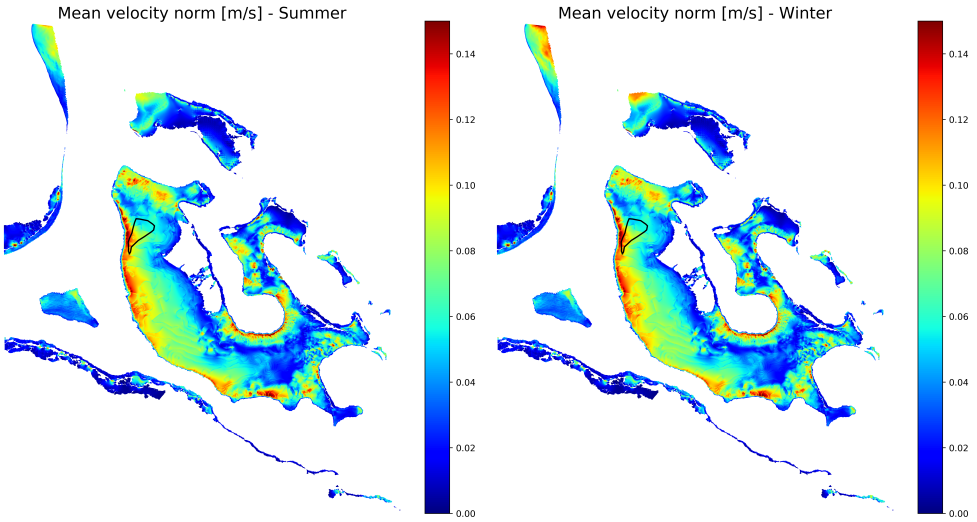

Fig. A.1: Standard deviation of velocity norm obtained using wetting-drying and $C_S = 5$ for summer and winter 2016

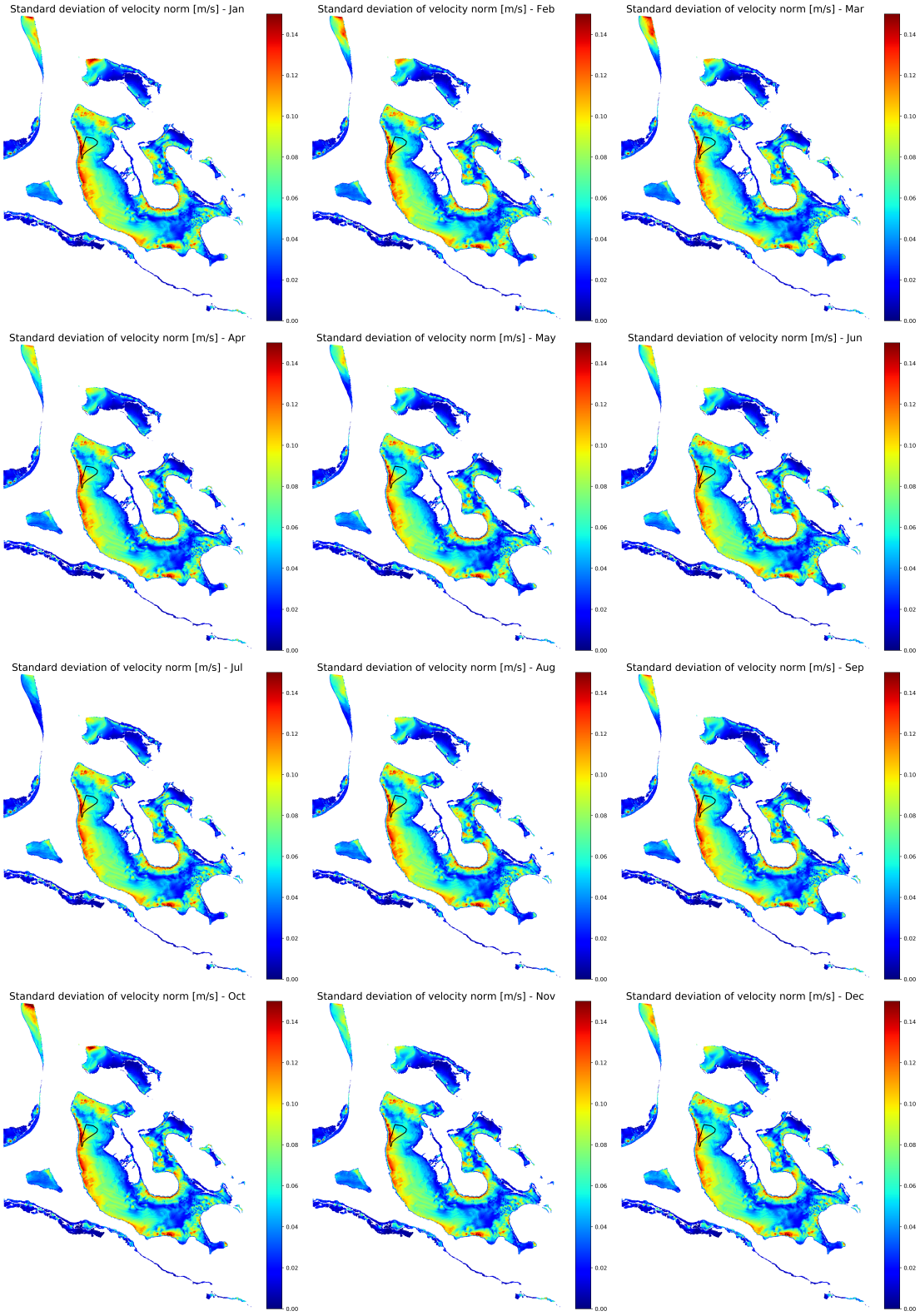

Fig. A.2: Standard deviation of velocity norm obtained using wetting-drying and $C_S = 5$ (2016)

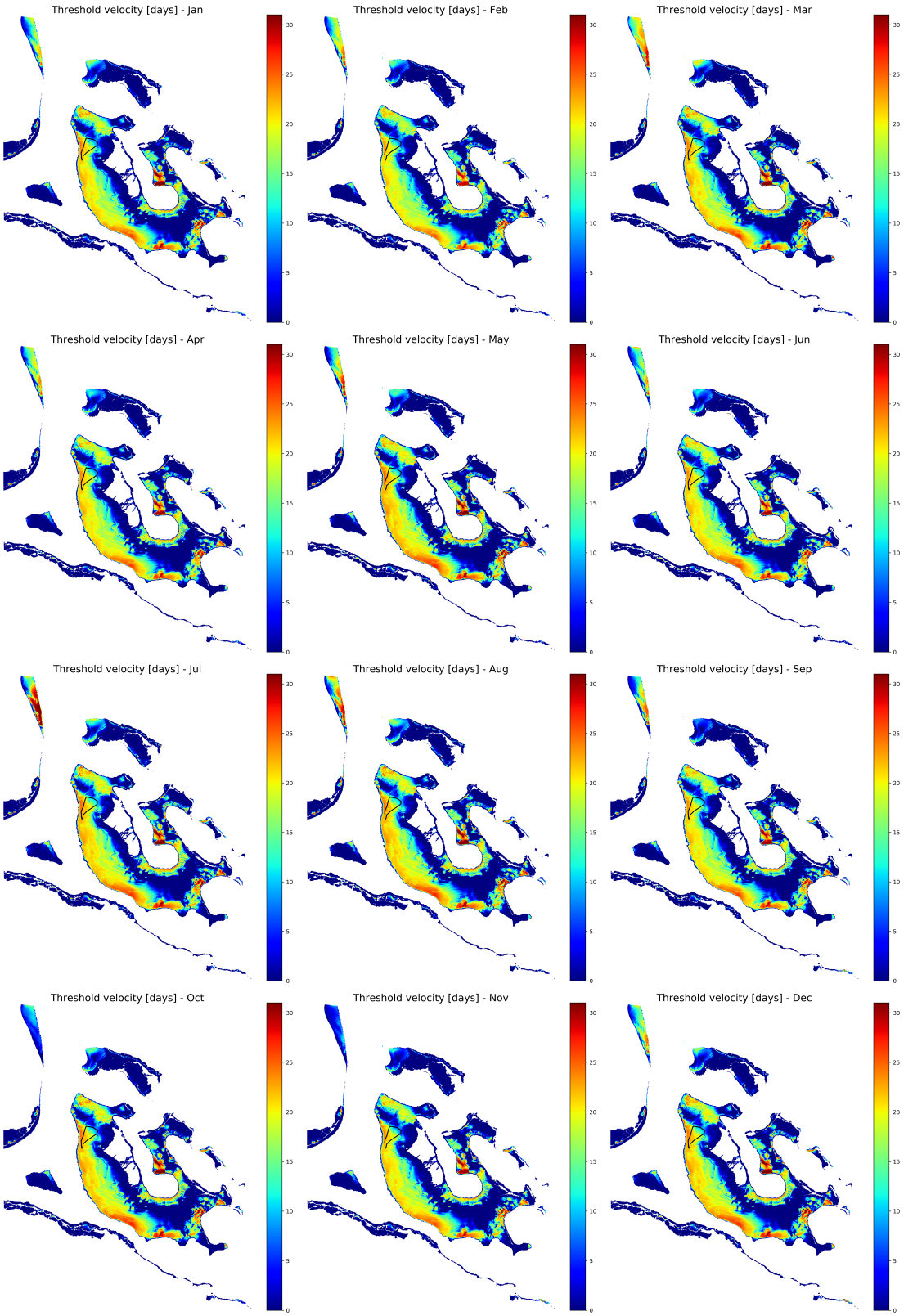

Fig. A.3: Threshold velocity indicator obtained using wetting-drying and $C_S = 5$ (2016)

Rue Archimède, 1 bte L6.11.01, 1348 Louvain-la-Neuve **www.uclouvain.be/epl**

